A model for the spreading and compaction of two-phase viscous gravity currents

CHLOÉ MICHAUT† AND DAVID BERCOVICI

Department of Geology and Geophysics, Yale University, New Haven, CT 06520-8109, USA

Two-phase viscous gravity current theory has numerous applications in the natural sciences, from small-scale lava, sedimentary and glacial flows, to large-scale flows of partially molten mantle. We develop the general equations for two-phase viscous gravity currents composed of a high viscosity matrix and low viscosity fluid for both constant volume and constant flux conditions. A loss of fluid phase is taken into account at the current's upper boundary and corresponds to the degassing of a lava flow or loss of water in sedimentary flows. As the current spreads, its surface increases and fluid loss is facilitated, which modifies the mixture density and viscosity and thus the current's shape; hence spreading of the flow affects fluid loss and vice-versa. Our results show that two-phase gravity currents retain and transport the fluid out to large distances, but the fluid is almost entirely lost within a region of finite radius. This 'loss radius' depends on the flow's volume or flux, fluid and matrix properties as well as on the size of fluid parcels or matrix permeability. Application to lava flows shows that degassing occurs over a large area, which affects gas release and transport in the atmosphere.

---

1. Introduction

Low-Reynolds-number gravity currents propagating over a rigid horizontal surface involve the spreading of a viscous material under its own weight. Viscous gravity current theory has numerous applications in geosciences, from the small to intermediate scale emplacement of lava, mud and ice flows, to the large-scale flow of mantle plume heads, deformation of weak continental crust under its own weight and the flow of polar ice caps (Huppert 2006).

The propagation of an isothermal buoyant fluid of constant viscosity over a horizontal surface has been described in detail by Huppert (1982). Gravity currents in real geological settings are, however, very complex, geometrically and physically. Many geological gravity currents are comprised of viscous fluids with temperature-dependent viscosity and/or buoyancy and are also multi-component and multi-phase materials. This is the case for lava flows and plume-heads spreading beneath a rigid surface; in particular, as they spread, fluid cools and becomes more viscous and dense. Unlike isothermal or constant viscosity gravity currents, cooling currents with temperature-dependent viscosity or buoyancy are not self-similar and develop various morphologies as they flow (Stasiuk, Jaupart & Sparks 1993; Bercovici 1994;

---

† Present address: Institut de Physique du Globe de Paris, Université Paris VII Denis-Diderot, 4, Avenue de Neptune, 94100 St-Maur des Fossés, France. E-mail address for correspondence: michaut@ipgp.jussieu.fr

Bercovici & Lin 1996). Analogue experiments have been performed to study the effects of surface cooling and the formation of a solid crust on the spreading of viscous gravity currents, as well as the effects of cooling on the flow of fluid with temperature-dependent viscosity (Hallworth, Huppert & Sparks 1987; Crisp & Baloga 1990; Fink & Griffiths 1990; Griffiths & Fink 1993; Stasiuk *et al.* 1993).

In the case of a two-phase mixture of matrix and fluid, the spreading of the current is affected by the presence of a second phase. Jaupart (1991) demonstrated that a thick lava dome containing a compressible gas phase and characterized by a relatively high eruption rate and high viscosity behaves as a compressible fluid and flows less rapidly than its incompressible counterpart. The effects of the presence and settling of particles from high-Reynolds-number suspension gravity flows, such as pyroclastic flows, on the buoyancy and compressibility of the flow have been studied theoretically by Bonnecaze, Huppert & Lister (1993) and Timmermans, Lister & Huppert (2001). Particle-driven gravity currents have been described using the box model of Huppert & Simpson (1980), which considers the flow as a series of equal volume boxes of given shape (cylinder or rectangular) whose properties do not change horizontally (Bonnecaze *et al.* 1998; Hallworth, Huppert & Hogg 1998).

The emplacement of multi-component viscous gravity currents, such as lava or mud flows, involves a number of physical processes that cannot be studied with analogue experiments or single-phase fluid as usually considered (Huppert 1982; Jaupart 1991; Bercovici 1994). The presence of a second phase (gas in lava flows, water in mud flows, melt in mantle flows) modifies not only the compressibility, buoyancy and viscosity of the mixture, but generates interfacial forces that introduce strong complexity relatively to the single-phase theory. The density and pressure difference between the two phases cause relative motion between the phases and compaction of the matrix in more than just the vertical direction.

As the current spreads, its surface increases which facilitates the escape of the fluid phase. But as the current loses fluid, its physical properties, density and viscosity, change, which, in turn, modifies the spreading of the current. In this paper we examine how the spreading of a two-phase gravity current affects the loss of fluid and conversely, how the loss of fluid affects the spreading of the current.

Such complex two-phase flows cannot be treated simply with constant viscosity single-phase single-component flows and necessitate a more complete theory. The dynamics of two-phase media has been well studied. Two-phase theories with applications in magma dynamics (McKenzie 1984; Spiegelman 1993*a*, *b*, *c*), glaciology (Fowler 1984) or inner core growth (Sumita *et al.* 1996), are among the relevant theories for our study. We use the approach developed by Bercovici, Ricard & Schubert (2001*a*, *b*), Ricard, Bercovici & Schubert (2001) and Bercovici & Ricard (2003) because it explicitly accounts for a difference in pressure between phases, as well as surface tension and isotropic damage, i.e. the creation of interfacial energy by deformational work, which may be added later in the model.

In this paper we first develop the general equations for the gravitational spreading over a horizontal surface of an axisymmetric two-phase gravity current composed of viscous matrix and fluid. The matrix and fluid have different densities and are both incompressible; the matrix has a much higher viscosity than the fluid. As in the single-phase gravity current theory, we derive the integrated equations over the thickness of the flow, for the evolution of the current's thickness and volume fraction of fluid with time and radial coordinate. These equations take into account variations of the flow density and viscosity with fluid volume fraction, relative motions between fluid and matrix and the pressure difference between phases. A loss of

fluid phase is considered at the top of the flow as the fluid is less dense than the matrix.

Following the development of the general equations, we solve numerically the equations for both constant volume and constant volume–flux flows and propose different scaling laws. The shape of a two-phase viscous gravity current is shown to vary with the dependence of the mixture viscosity on the fluid volume fraction. We derive a characteristic time for fluid loss as a function of the fluid and matrix physical properties and volume or flux of the flow. We also find a characteristic thickness for a significant fluid loss and a characteristic radius over which fluid loss occurs.

Finally, we apply these results to describe the degassing of different types of lava flows, in particular flood basalt events. Indeed, such large lava flows have released large quantities of gas into the Earth's atmosphere and might have had a large impact on the atmosphere composition and circulation (Self, Widdowson & Jay 2006). Explosive eruptions of lava and gas mixtures release buoyant hot gas directly at the vent. Large explosive basaltic eruptions might release hot gas and tephras in the lower stratosphere, that are then transported by stratospheric winds (Thordarson & Self 1993). Giant ash clouds generated by super-eruptions of felsic lavas can spread within the stratosphere, and reach radii at which they become sensitive to Coriolis forces, generating cyclonic features (Baines & Sparks 2005). Effusive eruptions, however, lead to the transport of gas within the lava, and to its release far from the vent, with less buoyancy, implying a different mode of transport of gas into the atmosphere; as flood basalt lava flows may spread over several hundreds and even thousands of kilometres (Ho & Cashman 1997), this effect may be important. The time scale and surface area over which processes such as lava emplacement and degassing occur influence atmospheric composition and dynamics. For example, for such high volume flows, the radius over which degassing occurs may approach the Rossby radius of deformation (Gill 1982), leading to a possible cyclonic activity.

2. Theory
2.1. *Introduction to the theory*

The equations for the spreading of a two-phase gravity current are derived from the equations of motion and mass conservation for a two-phase mixture. We consider two different cases for the flow of mixture: a flow of suspended fluid particles within matrix and Darcy flow of porous matrix with connected pores full of fluid. In the second case, a pressure difference exists between the two phases. However, we show that this pressure difference has no effect on fluid loss as long as the compaction length, i.e. the extent over which the matrix collapses and fluid is expelled under an applied compressive load, is smaller than the flow thickness. We derive the equations of motion in this simple physical limit for Darcy flow, and in the general case for a suspension flow. The final equations governing the evolution of the thickness h and vertically averaged volume fraction of fluid ϕ of the gravity current will be given in their dimensional and dimensionless forms.

Following this analysis, the non-dimensionalization of the equations shows that, for most natural flows, these complex equations can be reduced to a simpler form as the horizontal separations of the phase can in general be neglected in comparison with the terms of spreading and degassing. The reduced equations are solved numerically and results are analysed in a separate section.

2.2. *Equations of motion*

We consider an axisymmetric gravity current composed of a mixture of two phases, matrix and fluid, spreading over a horizontal surface. Matrix and fluid are both incompressible but have different physical properties. The theoretical averaging model of Bercovici *et al.* (2001*a*), Ricard *et al.* (2001) and Bercovici & Ricard (2003) is used to describe the dynamics of a simple two-phase mixture undergoing creeping flow, i.e. for which inertia and acceleration are negligible.

2.2.1. *Mass conservation*

Mass conservation of fluid and matrix assumed incompressible gives

$$\frac{\partial \varphi}{\partial t} + \nabla \cdot \varphi \boldsymbol{v}_f = 0, \tag{2.1}$$

$$\frac{\partial (1 - \varphi)}{\partial t} + \nabla \cdot (1 - \varphi) \boldsymbol{v}_m = 0, \tag{2.2}$$

where φ is the volume fraction of fluid, $\boldsymbol{v}$ is the velocity and subscript m stands for matrix and f for fluid. By addition of (2.1) and (2.2), we obtain

$$\nabla \cdot \bar{\boldsymbol{v}} = 0, \tag{2.3}$$

with $\bar{q} = (1 - \varphi)q_m + \varphi q_f$ and $\Delta q = q_m - q_f$, for any quantity q. Since $\boldsymbol{v}_m = \bar{\boldsymbol{v}} + \varphi \Delta \boldsymbol{v}$, then $\nabla \cdot \boldsymbol{v}_m = \nabla \cdot (\varphi \Delta \boldsymbol{v})$.

2.2.2. *Momentum equations*

The viscosity of the matrix μ_m is assumed much larger than the viscosity of the fluid μ_f, $(\mu_m \gg \mu_f)$. Creeping flow is valid for a two-phase medium even when the fluid phase is low viscosity as long as the fluid fraction is small and if the interaction drag force between fluid and matrix is high, due, for instance, to a low permeability. For this study, we neglect the treatment of damage and surface tension prescribed in the original theory of Bercovici *et al.* (2001*a*) and Bercovici & Ricard (2003).

The momentum equation for each phase is given by (Bercovici & Ricard 2003)

$$0 = -\varphi \left[\nabla P_f + \rho_f g z \right] + c \Delta \boldsymbol{v} \tag{2.4}$$

$$0 = -(1 - \varphi) \left[\nabla P_m + \rho_m g z \right] + \nabla \cdot \left[(1 - \varphi) \underline{\boldsymbol{\tau}}_m \right] - c \Delta \boldsymbol{v} + \Delta P \nabla \varphi, \tag{2.5}$$

where P represents pressure, g acceleration of gravity, ρ is density and c is the interfacial drag coefficient, which controls the resistance to relative movement between phases. The coefficient c may be a function of the fluid volume fraction and we assume that

$$c = c_0 \varphi^n, \tag{2.6}$$

where c_0 and n are constants; this assumption is valid if we consider either Darcy flow, in which the fluid forms an interconnected network, or a suspension flow, if the fluid phase is a suspension within the matrix. In the case of Darcy flow, McKenzie (1984) and Bercovici *et al.* (2001*a*) have shown that $c = \mu_f \varphi^2 / k$, with k the permeability. For tubule connections $k = k_0 \varphi^2$, where k_0 is a reference permeability; this gives $n = 0$ and $c_0 = \mu_f / k_0$ for Darcy flow. For suspension flow, we show in Appendix A, that $n = 1$ and $c_0 = 9\mu_m / 2r_b^2$, where r_b is the radius of the fluid particles in suspension (e.g. gas bubbles).

The quantity $\underline{\boldsymbol{\tau}}_m$ is the viscous stress tensor averaged over the volume of the matrix. Viscous stress associated with deformation of the fluid is negligible compared to pressure forces because of the low viscosity of the fluid relatively to that of the matrix.

As in all single-phase gravity current theories (Huppert 1982; Lister & Kerr 1989; Bercovici & Lin 1996), horizontal variations in stress and velocity are negligible compared to vertical variations. Radial motion is similar to the flow in a thin disc-like cylindrical channel, with a typical edge radius R much greater than the typical thickness H of the flow. For each phase $j = f$ or m, we write the velocity as $\boldsymbol{v}_j = (u_j, 0, w_j)$ in cylindrical coordinate, with $u_j \gg w_j$.

Viscous resistance is the primary force acting against the flow of material. A simple scaling analysis of (2.5) along the r-direction shows that the dynamic pressure P_m scales with $\mu_m U R / H^2$, where U is a characteristic radial velocity. The main component of the divergence of the stress tensor scales as $\mu_m W / H^2$ (where W is a vertical velocity scale and $W \ll U$); this is negligible in comparison with the vertical pressure gradient scale P_m / H, using the scaling for P_m provided above. Therefore, no component of the stress tensor remains in the vertical component of (2.5). Multiplying (2.4) by $(1 - \varphi)$ and subtracting the product of 2.5 by φ, we get

$$-\boldsymbol{\nabla}\left[(1 - \varphi)\Delta P\right] - (1 - \varphi)\Delta \rho g z + \frac{\partial}{\partial z}\left[(1 - \varphi)\mu_m \frac{\partial u_m}{\partial z}\right]\boldsymbol{r} - \frac{c}{\varphi}\Delta \boldsymbol{v} = 0, \qquad (2.7)$$

where u_m is the horizontal component of matrix velocity, and $\boldsymbol{r}$ and $\boldsymbol{z}$ the unit vectors in the radial and vertical directions, respectively.

In order to derive the equations which describe the evolution of thickness and fluid fraction, we seek the expressions for two horizontal components of the velocity, i.e. u_m and u_f, or alternatively u_m and Δu. This requires solving for the fluid and matrix pressure first.

2.2.3. *Pressure*

In the absence of damage and surface tension, the difference in pressure between the two phases arises from viscous resistance due to dilation and compaction. If we consider that the fluid phase forms a suspension, then there is no difference in pressure between the phases and we have $P = P_m = P_f$, $\Delta P = 0$. From (2.4) we obtain that $\Delta \boldsymbol{v} = \varphi(\boldsymbol{\nabla} P + \rho_f g z)/c$. No component of the stress tensor remains in the vertical component of (2.5) (see discussion in §2.2.2) and the sum of (2.4) and (2.5) gives

$$\frac{\partial P}{\partial z} = -\bar{\rho}g. \qquad (2.8)$$

As shown below, this equation is also valid for a permeable flow ($n = 0$) in the case where the typical thickness of the flow is larger than the vertical extent over which the matrix viscously deforms and compacts, because the difference in pressure ΔP between the phases is then negligible.

With the condition $\mu_f \ll \mu_m$, Bercovici & Ricard (2003) show that, for permeable flow

$$\Delta P = -\frac{K\mu_m}{\varphi}\boldsymbol{\nabla} \cdot \boldsymbol{v}_m, \qquad (2.9)$$

where K, a dimensionless factor accounting for pore or grain geometry, is typically of order 1.

For simplicity, we first consider that φ varies linearly as a function of z with a small variation θ/h.

$$\varphi = \phi + \frac{\theta}{h}\left(z - \frac{h}{2}\right), \qquad (2.10)$$

where $z = h$ corresponds to the surface of the matrix, ϕ is the average value for φ over the thickness of the flow and we assume $\theta \ll \phi$. We thus have $\partial\varphi/\partial z = \theta/h$ and $\varphi \sim \phi$ since $\theta \ll \phi$; the vertical variation of φ is thus negligible when integrating over z. Large variations of φ with z are examined in Appendix E.

Using (2.3), (2.4), (2.6) with $n = 0$ (permeable flow with permeability $k = k_0\phi^2$), (2.9) and for a typical edge radius R much greater than the typical thickness H, we obtain

$$\Delta P = -\frac{K\mu_m}{\varphi}\nabla\cdot(\varphi\Delta\mathbf{v}) = -\frac{K\mu_m}{c_0}\left[2\frac{\theta}{h}\left(\frac{\partial P_f}{\partial z} + \rho_f g\right) + \varphi\frac{\partial^2 P_f}{\partial z^2}\right]. \tag{2.11}$$

Replacing for ΔP in the vertical component of (2.7) and using (2.4) to express $c\Delta w$ as a function of P_f gives

$$(1-\varphi)\varphi\delta^2\frac{\partial^3 P_f}{\partial z^3} + (3-4\varphi)\frac{\theta}{h}\delta^2\frac{\partial^2 P_f}{\partial z^2} - \left(1 + 2\frac{\theta^2}{h^2}\delta^2\right)\frac{\partial P_f}{\partial z} - \bar{\rho}g - 2\frac{\theta^2}{h^2}\delta^2\rho_f g = 0, \tag{2.12}$$

where $\delta = (K\mu_m/c_0)^{1/2}$ is the viscous compaction length, i.e. the typical thickness over which viscous resistance to matrix squeezing occurs.

A simple scaling analysis emphasizes the importance of the different terms in (2.12) (though this equation is solved in the general case in Appendix B). A characteristic rate of vertical phase segregation may be given by $\Delta\rho g/c_0$ (see for instance (2.7)), and this is associated with a decrease in total thickness with time due to fluid loss noted $\dot{H}_f$. We can compare this fluid-loss collapse rate to that due to simple spreading by considering the thickness evolution for a single-phase gravity current (which, as shown later, is a limiting case for $\varphi \to 0$; Huppert (1982))

$$\frac{\partial h}{\partial t} = \frac{\rho_m g}{3\mu_m r}\frac{\partial}{\partial r}\left(h^3 r\frac{\partial h}{\partial r}\right). \tag{2.13}$$

The characteristic collapse rate due to spreading $\dot{H}_s$ is derived from (2.13) by scaling analysis, using the volume scale $V_0 = \pi H R^2$

$$\dot{H}_s \sim \frac{\rho_m g H^4}{\mu_m R^2} = \frac{\rho_m g H^5 \pi}{\mu_m V_0}. \tag{2.14}$$

Both collapse processes are significant and play a similar role when the rate of collapse due to spreading and the rate of collapse due to fluid loss are equivalent ($\dot{H}_s \sim \dot{H}_f$), i.e. when the thickness of the flow is

$$H \sim \left(\frac{V_0\Delta\rho\mu_m}{\pi\rho_m c_0}\right)^{1/5}. \tag{2.15}$$

By scaling vertical derivatives with $1/H$ and h with H in (2.12), we obtain

$$\nu^2(1-\varphi)\varphi\frac{P_f}{H} + \nu^2(3-4\varphi)\theta\frac{P_f}{H} - (1 + 2\theta^2\nu^2)\frac{P_f}{H} - \bar{\rho}g - 2\theta^2\nu^2\rho_f g = 0, \tag{2.16}$$

with $\nu = \delta/H$.

For this analysis, we consider flows for which the compaction length δ is smaller than the characteristic thickness H, such that $\nu^2 = \delta^2/H^2 \ll 1$. As demonstrated later in the paper (see §§2.4 and 5.1.2), this assumption is relevant for most two-phase viscous flows in nature. Thus, given $\nu^2 \ll 1$, only two terms in (2.16) remain, which yield

$$\frac{\partial P_f}{\partial z} = -\bar{\rho}g. \tag{2.17}$$

Thus, as in the single-phase theory, the hydrostatic assumption is a good approximation for the fluid's vertical pressure gradient in a two-phase viscous gravity current for which $\nu^2 \ll 1$ (see Appendix B for more details).

We have then, for $\theta \ll \phi$,

$$P_f = P_a + \bar{\bar{\rho}}g(h-z), \tag{2.18}$$

where P_a is the ambient pressure at $z = h$ and $\bar{\bar{q}} = (1-\phi)q_m + \phi q_f$, for any quantity q. Using (2.17) in (2.11) gives an estimate for ΔP

$$\Delta P \sim \Delta \rho g H \frac{\delta^2}{H^2} \frac{\theta}{h/H}(2 - 3\phi), \tag{2.19}$$

and thus $\Delta P \ll P_f$ for $\nu^2 = \delta^2/H^2 \ll 1$, which shows that viscous resistance to compaction is not the limiting mechanism for fluid loss; the loss of fluid is controlled by fluid escape by buoyant permeable Darcy flow rather than by matrix squeezing. If the compaction length were of the same order of magnitude as, or larger than, the characteristic thickness H, ΔP would be non-negligible and the loss of fluid at the surface of the current would be limited by viscous resistance to matrix deformation (see Appendix B).

2.2.4. *Horizontal velocities*

Given that ΔP is negligible relative to P_f, one can readily derive the expression for the radial velocities u_m and Δu using the expression of P_f (2.18), valid for both Darcy (considering and $\nu^2 \ll 1$) and Stokes flows, with $\varphi \sim \phi$. Note that only the average value of the volume fraction of fluid remains in the equation, and vertical variations of porosity are negligible. The radial component of (2.5) becomes

$$\mu_m \frac{\partial}{\partial z}\left((1-\phi)\frac{\partial u_m}{\partial z}\right) = \frac{\partial P_f}{\partial r} = \bar{\bar{\rho}}g\frac{\partial h}{\partial r} - \Delta \rho g(h-z)\frac{\partial \phi}{\partial r}. \tag{2.20}$$

To obtain an expression for u_m, a free-slip boundary condition is used at the surface of the current $z = h$. This condition is appropriate for gravity currents occurring at the surface of the Earth, such as lava flows, or if the viscosity of the surrounding fluid is less than or not greatly different from the current viscosity (Huppert 1982). Using the boundary conditions $\partial u_m/\partial z = 0$ at $z = h$, $u_m = 0$ at $z = 0$, and integrating (2.20) twice we obtain

$$u_m = \frac{g}{(1-\phi)\mu_m}\left[\bar{\bar{\rho}}\frac{\partial h}{\partial r}\left(\frac{z^2}{2} - hz\right) - \Delta \rho \left(-\frac{z^3}{6} + \frac{hz^2}{2} - \frac{h^2 z}{2}\right)\frac{\partial \phi}{\partial r}\right]. \tag{2.21}$$

For $\phi = 0$ (2.21) gives the expression for the radial velocity in a single-phase gravity current.

Similarly, the radial component of (2.4) gives an expression for Δu, with $c = c_0 \varphi^n$

$$\Delta u = \frac{\phi^{1-n}}{c_0}\frac{\partial P_f}{\partial r} = \phi^{1-n}\frac{g}{c_0}\left[\bar{\bar{\rho}}\frac{\partial h}{\partial r} - \Delta \rho(h-z)\frac{\partial \phi}{\partial r}\right]. \tag{2.22}$$

In both (2.21) and (2.22), the variations in fluid and matrix velocities result from radial gradients in thickness and volume fraction of fluid.

2.3. *Shape and volume fraction of fluid*

As for the single-phase gravity current theory, we apply the conservation of mass for both phases to derive the evolution of current thickness and volume fraction of fluid.

We consider the general case of a fluid phase less dense than the matrix ($\rho_f < \rho_m$), and a matrix denser than the environment, such that the fluid ascends relative to the matrix and fluid loss occurs at the upper deformable boundary of the current, $z = h(r, t)$. We also consider the possibility of injection of mixture of fluid and matrix with a fixed volume fraction of fluid ϕ_0 into the current through the lower boundary ($z = 0$) at a given vertical velocity W. For simplicity, the velocity W is equal for both fluid and matrix and depends only on r.

Conservation of the masses of fluid and matrix give, for $\theta \ll \phi$,

$$\frac{\partial}{\partial t}\left[2\pi r \int_0^h \phi\,\mathrm{d}z\right]\mathrm{d}r = -\frac{\partial}{\partial r}\left[2\pi r \int_0^h \phi u_f\,\mathrm{d}z\right]\mathrm{d}r + \phi(2\pi r\,\mathrm{d}S)\boldsymbol{n}\cdot\Delta\boldsymbol{v}|_{z=h}$$
$$+ 2\pi r\phi_0 W(r)\,\mathrm{d}r \tag{2.23}$$

$$\frac{\partial}{\partial t}\left[2\pi r \int_0^h (1-\phi)\,\mathrm{d}z\right]\mathrm{d}r = -\frac{\partial}{\partial r}\left[2\pi r \int_0^h (1-\phi)u_m\,\mathrm{d}z\right]\mathrm{d}r$$
$$+ 2\pi r(1-\phi_0)W(r)\,\mathrm{d}r, \tag{2.24}$$

where $2\pi r\,\mathrm{d}S$ is the area of the incremental surface over which the fluid is lost and $\boldsymbol{n}$ is the vector normal to the surface. The term proportional to $\Delta\boldsymbol{v}$ represents fluid loss (fluid velocity relative to matrix velocity at the surface). Equations (2.23) and (2.24) are equivalent to the integrated form of (2.1) and (2.2) over the thickness of the current.

One can readily show that

$$\mathrm{d}S\boldsymbol{n}\cdot\Delta\boldsymbol{v}|_{z=h} = \Delta w|_{z=h}\mathrm{d}r + \frac{\partial h}{\partial r}\Delta u|_{z=h}\,\mathrm{d}r. \tag{2.25}$$

By addition of (2.23) and (2.24) and simplification of (2.24), we obtain the following equations in the general case:

$$\frac{\partial h}{\partial t} = -\frac{1}{r}\frac{\partial}{\partial r}\left[r\int_0^h (u_m - \phi\Delta u)\,\mathrm{d}z\right] + \phi\left[\Delta w + \frac{\partial h}{\partial r}\Delta u\right] + W(r) \tag{2.26}$$

$$\frac{\partial((1-\phi)h)}{\partial t} = -\frac{1}{r}\frac{\partial}{\partial r}\left[r\int_0^h (1-\phi)u_m\,\mathrm{d}z\right] + (1-\phi_0)W(r). \tag{2.27}$$

Taking into account fluid loss in the equations requires the expression for Δw at the surface of the matrix. Considering $\nu^2 \ll 1$ and $\theta \ll \phi$, (2.4) and (2.17) give

$$\Delta w(z = h) = -\frac{\Delta\rho g}{c_0}\phi^{1-n}(1-\phi), \tag{2.28}$$

which is valid for both Darcy and suspension flows with $n = 0$ or $n = 1$. (Again, large variations of φ with z are examined in Appendix E for Darcy flow.)

Using expressions (2.21) and (2.22) for u_m and Δu and combining (2.26) and (2.27), we obtain the following equations for the evolutions of the thickness and average volume fraction of fluid of the current with time and radial coordinate, using $\nu^2 \ll 1$ for Darcy flow and $\theta \ll \phi$:

$$\frac{\partial h}{\partial t} = \frac{g}{r\mu_m}\frac{\partial}{\partial r}\left[\frac{\bar{\rho}h^3 r}{3(1-\phi)}\frac{\partial h}{\partial r} - \frac{\Delta\rho h^4 r}{8(1-\phi)}\frac{\partial\phi}{\partial r}\right] + \frac{g}{rc_0}\frac{\partial}{\partial r}\left[\bar{\bar{\rho}}\phi^{2-n}hr\frac{\partial h}{\partial r}\right.$$
$$\left.-\frac{\Delta\rho\phi^{2-n}h^2 r}{2}\frac{\partial\phi}{\partial r}\right] + W(r) - \frac{g\phi^{2-n}}{c_0}\left[\Delta\rho(1-\phi) - \bar{\bar{\rho}}\left(\frac{\partial h}{\partial r}\right)^2\right] \tag{2.29}$$

$$\frac{\partial \phi}{\partial t} = \frac{g}{\mu_m} \frac{\partial \phi}{\partial r} \left[\frac{\bar{\bar{\rho}} h^2}{3(1-\phi)} \frac{\partial h}{\partial r} - \frac{\Delta \rho h^3}{8(1-\phi)} \frac{\partial \phi}{\partial r} \right] + \frac{g}{c_0} \frac{(1-\phi)}{rh} \frac{\partial}{\partial r} \left[\bar{\bar{\rho}} \phi^{2-n} hr \frac{\partial h}{\partial r} \right.$$

$$\left. - \frac{\Delta \rho \phi^{2-n} h^2 r}{2} \frac{\partial \phi}{\partial r} \right] + \frac{(\phi_0 - \phi)}{h} W(r) - \frac{g \phi^{2-n}(1-\phi)}{c_0 h} \left[\Delta \rho (1-\phi) - \bar{\bar{\rho}} \left(\frac{\partial h}{\partial r} \right)^2 \right],$$

$$(2.30)$$

where $\bar{\bar{\rho}} = (1-\phi)\rho_m + \phi \rho_f$, and $n = 1$ for suspensions or $n = 0$ for Darcy flow.

Both evolution equations are composed of four different parts. The first term on the right-hand side of each equation represents changes of thickness or fluid fraction due to current spreading; horizontal phase separation leads to the second term on the right-hand side. Both spreading and phase separation are governed by radial gradients in thickness and fluid fraction. The third term is a source term, which is used in the case where material is injected into the current through one of its boundaries. The fourth and last term represents the loss of fluid through the surface of the current.

When $\phi = 0$, the only remaining term in (2.29) corresponds to the single-phase theory.

2.4. *Constant volume versus constant flux*

There are two classic cases of gravity currents representing isolated masses or masses fed by injection of material. These are called constant volume currents or constant flux currents. The net volume flux into the current is

$$Q = 2\pi \int_0^\infty Wr \, \mathrm{d}r \qquad (2.31)$$

which we assume constant. For simplicity, the velocity of injected material W is defined to be a Gaussian function of r, centred at $r = 0$, with half-width a

$$W(r) = \frac{Q}{\pi a^2} \mathrm{e}^{-r^2/a^2}. \qquad (2.32)$$

Employing this source function allows us to examine the effects of the characteristic size of the source a on the current's shape and on fluid loss. In the limit $a \to 0$ (2.32) is equivalent to the point-source boundary condition $h(0) \to \infty$, as used by Huppert (1982) for a single-phase gravity current. The net volume of matrix is obtained by integrating its thickness over the area

$$2\pi \int_0^\infty (1-\phi)hr \, \mathrm{d}r = (Qt + V_0)(1 - \phi_0), \qquad (2.33)$$

where V_0 is the initial volume of the current and $Q = 0$ for constant volume currents.

2.5. *Non-dimensionalization*

The dimensional governing equations for a two-phase viscous gravity current are (2.29) and (2.30) for $\nu^2 \ll 1$ and $\theta \ll \phi$. We non-dimensionalize these equations using a vertical scale H, a radial scale R and a time scale T given by

$$H = \begin{cases} \left(\dfrac{V_0 \Delta \rho \mu_m}{\pi \rho_m c_0} \right)^{1/5} & \text{if } Q = 0 \\[4mm] \left(\dfrac{Q \mu_m}{\pi \rho_m g} \right)^{1/4} & \text{if } Q > 0 \end{cases} \qquad (2.34)$$

$$
T = \frac{c_0 H}{\Delta \rho g} =
\begin{cases}
\dfrac{1}{g} \left(\dfrac{V_0 \mu_m c_0^4}{\pi \rho_m \Delta \rho^4} \right)^{1/5} & \text{if } Q = 0 \\[3mm]
\dfrac{c_0}{\Delta \rho g} \left(\dfrac{Q \mu_m}{\pi \rho_m g} \right)^{1/4} & \text{if } Q > 0
\end{cases}
\tag{2.35}
$$

$$
R =
\begin{cases}
\left(\dfrac{V_0}{\pi H} \right)^{1/2} = \left(\dfrac{V_0^4 c_0 \rho_m}{\pi^4 \Delta \rho \mu_m} \right)^{1/10} & \text{if } Q = 0 \\[3mm]
\left(\dfrac{QT}{\pi H} \right)^{1/2} = \left(\dfrac{Q c_0}{\pi \Delta \rho g} \right)^{1/2} & \text{if } Q > 0
\end{cases}
\tag{2.36}
$$

These different scales are defined by equating the non-dimensional groups in front of the terms of spreading and loss of fluid to 1. We also use $\pi R^2 H = V_0$ if $Q = 0$, or $\pi R^2 H = QT$ if $Q > 0$. These scales are all functions of the volume or volume flux of the flow and they almost all involve physical parameters characterizing both phases. Only H for $Q > 0$ involves physical properties of the matrix only. In this case, H is the vertical scale as defined for the single-phase flow (Huppert 1982), suggesting that the vertical scale is not influenced by the loss of fluid for $Q > 0$.

The dimensionless governing equations thus become

$$
\frac{\partial h}{\partial t} = \frac{1}{r} \frac{\partial}{\partial r} \left[\frac{(1 - \beta \phi) h^3 r}{3(1 - \phi)} \frac{\partial h}{\partial r} - \frac{\beta h^4 r}{8(1 - \phi)} \frac{\partial \phi}{\partial r} \right] + \frac{\sigma}{r} \frac{\partial}{\partial r} \left[\frac{(1 - \beta \phi)}{\beta} \phi^{2-n} h r \frac{\partial h}{\partial r} \right.
$$
$$
\left. - \frac{\phi^{2-n} h^2 r}{2} \frac{\partial \phi}{\partial r} \right] + \frac{1}{\gamma^2} e^{-r^2/\gamma^2} - \phi^{2-n} \left[(1 - \phi) - \sigma \frac{(1 - \beta \phi)}{\beta} \left(\frac{\partial h}{\partial r} \right)^2 \right] \tag{2.37}
$$

$$
\frac{\partial \phi}{\partial t} = \frac{\partial \phi}{\partial r} \left[\frac{(1 - \beta \phi) h^2}{3(1 - \phi)} \frac{\partial h}{\partial r} - \frac{\beta h^3}{8(1 - \phi)} \frac{\partial \phi}{\partial r} \right] + \sigma \frac{(1 - \phi)}{rh} \frac{\partial}{\partial r} \left[\frac{(1 - \beta \phi)}{\beta} \phi^{2-n} h r \frac{\partial h}{\partial r} \right.
$$
$$
\left. - \frac{\phi^{2-n} h^2 r}{2} \frac{\partial \phi}{\partial r} \right] + \frac{(\phi_0 - \phi)}{h} \frac{1}{\gamma^2} e^{-r^2/\gamma^2} - \frac{(1 - \phi) \phi^{2-n}}{h}
$$
$$
\times \left[(1 - \phi) - \sigma \frac{(1 - \beta \phi)}{\beta} \left(\frac{\partial h}{\partial r} \right)^2 \right], \tag{2.38}
$$

where

$$
\beta = \frac{\Delta \rho}{\rho_m} \tag{2.39}
$$

$$
\nu = \frac{\delta}{H} \tag{2.40}
$$

$$
\gamma = \frac{a}{R} \quad \text{if } Q > 0 \tag{2.41}
$$

$$
\sigma = \frac{H^2}{R^2} =
\begin{cases}
\left(\dfrac{\mu_m \Delta \rho}{c_0 \rho_m} \right)^{3/5} \left(\dfrac{\pi}{V_0} \right)^{2/5} & \text{if } Q = 0 \\[3mm]
\dfrac{\Delta \rho g}{c_0} \left(\dfrac{\pi \mu_m}{Q \rho_m g} \right)^{1/2} & \text{if } Q > 0
\end{cases}
\tag{2.42}
$$

All the variables in (2.37)–(2.42) hereafter are dimensionless. If the characteristic separation velocity is larger than the spreading velocity, then $\sigma > 1$ and the fluid flows more rapidly horizontally than the matrix spreads and escapes at the edge of the current. Once fluid is lost the layer spreads like a single-phase gravity current.

If the spreading velocity is larger than the separation velocity, then $\sigma < 1$, and the matrix spreads faster than fluid escapes. The current progressively loses its fluid phase through the upper surface.

For most natural two-phase viscous gravity currents, for example lava flows (see §5), $H^2/R^2 = \sigma \ll 1$. As the current spreads, its surface increases, which facilitates fluid loss. And as fluid is lost, the average density $\bar{\rho}$ of the current increases, which facilitates the spreading, but the average viscosity of the current $(1 - \phi)\mu_m$ also increases which acts adversely to flow. The effect of a different rheology for the flow is examined in Appendix D using different functions for the variations of the effective viscosity with the fraction of fluid.

Since ν is

$$\nu = \frac{(K\mu_m/c_0)^{1/2}}{H} = \left(\frac{K\sigma}{\beta}\right)^{1/2} \tag{2.43}$$

and K is of the order of 1, $\beta \sim 1$, assuming $\sigma \ll 1$, gives $\nu^2 \ll 1$. And hence the hydrostatic assumption for the vertical pressure gradient in the current is valid. The effects of viscous compaction are studied in Appendix B.

In the calculations we develop for constant volume and constant volume flux two-phase gravity currents, we consider $\sigma \ll 1$ and $\nu \ll 1$.

2.6. *Boundary and initial conditions*

If we assume there are no point sources of mass of fluid and matrix, then $a \neq 0$ and both thickness h and volume fraction of fluid ϕ are continuous at $r = 0$. At $r = 0$, symmetry requires

$$\frac{\partial h}{\partial r} = \frac{\partial \phi}{\partial r} = 0$$

for (2.37) and (2.38).

At $t = 0$, for $V_0 > 0$, the initial shape of h is defined such that

$$2\pi \int_0^\infty hr \, \mathrm{d}r = 1 \tag{2.44}$$

in which fluid loss has not yet occurred. The initial shape of the current is chosen to match the shape of a single-phase gravity current (Huppert 1982)

$$h(r, t = 0) = \begin{cases} \frac{4}{3\pi r_0^2}\left(1 - \frac{r^2}{r_0^2}\right)^{1/3} & \text{if } r \leqslant r_0 \\ 0 & \text{if } r > r_0 \end{cases} \tag{2.45}$$

where we choose $r_0 = 0.1$. Different initial shapes have been tested, including triangular or elliptical shapes. The shape of the current returns to the self-similar shape described by (2.45) in a dimensionless time of less than 5×10^{-8}. Moreover, the initial shape has no consequence on the fluid loss. The initial volume fraction of fluid is uniform and equal to ϕ_0 throughout the current for $r \leqslant r_0$; it is equal to zero outside the current for $r > r_0$.

Equations (2.37) and (2.38) are solved numerically using the finite-volume method of Patankar (1980); details on the numerical methods are given in Appendix C.

3. Constant volume gravity currents

In this section, we show the results of our calculations for the spreading and loss of fluid of a constant volume gravity current, i.e. $Q = 0$, using $\sigma \ll 1$ and $\nu \ll 1$ and
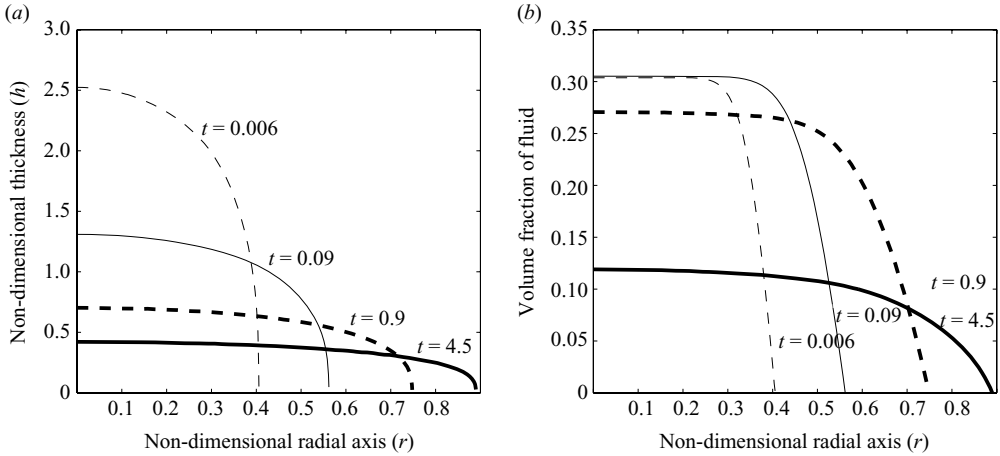
FIGURE 1. (a) Thickness and (b) volume fraction of fluid of a two-phase gravity current as a function of radial direction r at four different times. Parameters are dimensionless. $\phi_0 = 30\,\%$, $Q = 0$, $\beta = 0.98$, $\sigma \ll 1$, $\nu \ll 1$

considering permeable as well as suspension flows. Details on the numerical analysis are given in Appendix C.

3.1. *Thickness and fluid fraction profiles*

As the gravity current spreads and loses fluid, its shape remains essentially self-similar (figure 1*a*) and cannot be differentiated from the shape of a single-phase gravity current if the current viscosity is proportional to the average matrix fraction, and goes as $\mu_m(1 - \phi)$ (see Appendix D, figure 10). The current also remains similar for different values of ϕ_0. The shape of the current differs from a single-phase gravity current if the viscosity dependence on fluid volume fraction is different (see Appendix D).

The volume fraction of fluid drops predominantly because of buoyant escape through the surface and not by collapse of the current, and hence, the loss is small initially, when the surface area is small. Between $t = 0.006$ and $t = 0.9$, there is almost no fluid loss, and the fluid fraction averaged over the current's volume remains practically constant. The volume fraction of fluid is initially constant over r. The fluid fraction at the centre increases slightly at first because, with the large initial negative gradient in ϕ at the current's edge, the mixture weight, and hence the hydrostatic pressure, increase towards the edge; this effect drives a Darcy flux of fluid towards the centre (relative to the outwardly spreading matrix; see (2.22)) that causes fluid to accumulate briefly near the current's centre.

Fluid loss becomes larger as the current spreads and its surface increases. Indeed, later on, between $t = 0.9$ and $t = 4.5$, the current is more exposed, its surface is larger and the fluid fraction decreases substantially over the whole radius (figure 1*b*).

Far from the front, the radial gradient in ϕ stays very small and almost equal to zero, at any time.

3.2. *Evolution of fluid fraction, thickness and edge radius*

Our calculations show that the evolution of fluid fraction over time is identical for a given value of ϕ_0, and for $\sigma \ll 1$, $\nu \ll 1$ and $0.1 < \beta < 1$. Apart from the influence of ϕ_0, slight variations in the evolution of thickness and edge radius are induced by varying β, which we shall return to later in the paper. A different dependence of the
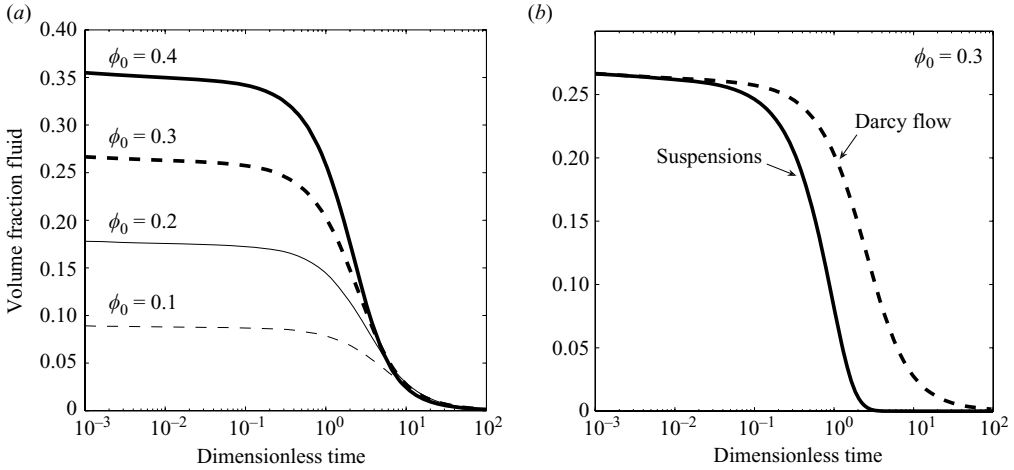
FIGURE 2. Evolution of the average fluid fraction $\langle \phi \rangle$ in the current as a function of dimensionless time. Fluid is lost at the surface of the flow. The higher the initial fluid content, the higher the rate of fluid loss. (*a*) Darcy flow, for four different initial fluid contents: $\phi_0 = 0.1$, 0.2, 0.3 and 0.4. (*b*) Suspension flow (solid line), Darcy flow is also indicated in dashed line, $\phi_0 = 0.3$. In both cases results are for $\sigma \ll 1$, $\nu \ll 1$ and $0.1 < \beta < 1$.

current's viscosity on fluid volume fraction does not significantly affect fluid loss (see Appendix D).

The evolution of the average fluid fraction in the current $\langle \phi \rangle$ with time shows that the loss of fluid accelerates at $t \sim 1$ (figure 2*a*). The higher the initial fluid content the higher the rate of fluid loss. When $\langle \phi \rangle$ attains very small values, close to 0.01, fluid loss becomes very slow and almost ceases. A surprising result is that the time scale for almost complete fluid loss is identical regardless of the initial fluid content. In all cases a value of $\langle \phi \rangle \sim 0.02$ is attained in $\sim 10T$, and a value of 0.01 is attained in $\sim 20T$, where T is the characteristic time scale given by (2.35), for $Q = 0$ and $c_0 = \mu_f / k_0$.

Fluid loss is proportional to the separation velocity at the surface ($\Delta w(z = h) \propto (1 - \phi) \times \phi^{1-n}$, $n = 0, 1$) and to the area over which fluid is lost, which is the dimensionless area of the current S times the volume fraction of fluid ϕ. Total fluid loss is thus proportional to $S \times (1 - \phi)\phi^{2-n}$, which increases with ϕ between 0 and 0.5. This explains why the higher the initial fluid volume fraction and the larger the surface of the current, the higher the rate of fluid escape.

In the suspension case the rate of fluid loss depends on ϕ, rather than ϕ^2 for Darcy flow, thus fluid loss is more rapid in dimensionless units, but the characteristic time scales are different in both cases. Fluid loss accelerates for $t \sim 0.1$ and it is complete in $t \sim 2T$, where T is the characteristic time scale given by (2.35), for $Q = 0$ and $c_0 = 9\mu_m / 2r_b^2$ (figure 2*b*).

Fluid loss affects the spreading of the current, as apparent on the evolution of the current's maximum thickness and edge radius (figures 3*a* and 3*b* for Darcy flow). Results are similar for the suspension case. The curves for different initial fluid fraction are compared with the case of a single-phase viscous gravity current, $\phi_0 = 0$. For a single-phase gravity current, Huppert (1982) shows that $h_d(\eta, t) = (3V_0\mu_m / \bar{\rho}g)t_d^{-1/4}f(\eta)$, where h_d and t_d are the dimensional thickness and time, respectively, η a similarity variable and $f(\eta)$ is a shape function. Similarly the edge radius is $r_d \propto t_d^{1/8}$.
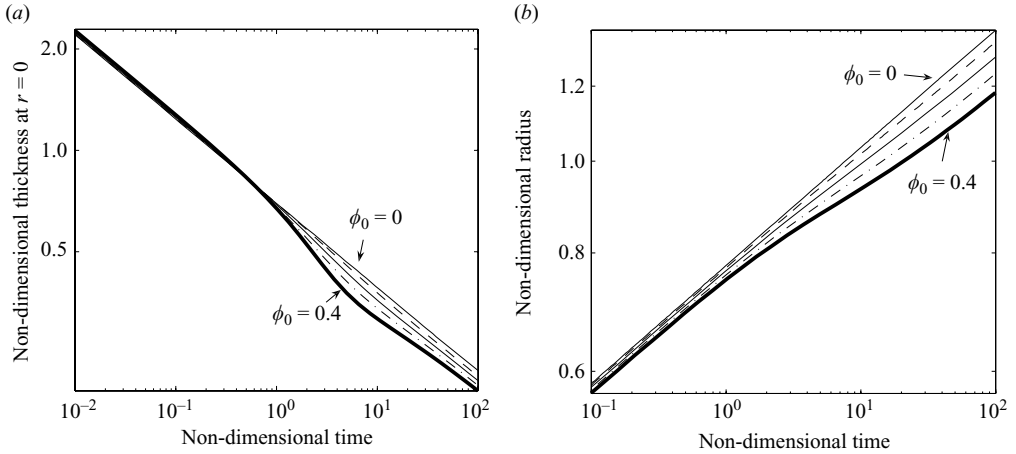
(*a*)

(*b*)

FIGURE 3. Evolution of dimensionless thickness h at $r = 0$ (*a*) and edge radius (*b*) as a function of dimensionless time for different values of the initial volume fraction of fluid ϕ_0 equal to 0 (solid line, indicated), 0.1 (dashed line), 0.2 (solid line), 0.3 (dash-dotted line) and 0.4 (bold line), considering Darcy flow. The case of a single-phase gravity current corresponds to $\phi_0 = 0$. These results are for $\sigma \ll 1$, $\nu \ll 1$ and $\beta = 0.98$.

The evolutions of the thickness and edge radius of a two-phase gravity current first parallel the single-phase ones (figure 3). The calculations all start with the same initial thickness and radius. When $t > 0.5$, fluid loss is significant. The effect of the fluid-loss event is apparent on the radius and thickness evolutions, both of which deviate significantly from the single-phase evolution. The higher the initial fluid fraction, the faster the decrease in thickness and the slower the increase in edge radius. This behaviour reflects the loss of fluid and overall loss of volume. Fluid loss becomes significant as the maximum thickness $h(r = 0) \rightarrow 1$. It occurs for $h(r = 0)$ varying between about 1 and 0.4, i.e. h close to 1, which verifies our assumption of $\delta/h < 0.1$ during fluid loss.

When dimensionless t becomes larger than 10–20, fluid loss is almost complete and has no more effect on the spreading of the current (figure 3). Indeed, after this time, the curves parallel the single-phase thickness and edge radius evolutions, with $h \propto t^{-1/4}$ and $r \propto t^{-1/8}$.

3.3. *Scaling analysis for maximum thickness and fluid fraction*

Far from the edge of the current, ϕ varies only slightly with r (figure 1*b*). We propose here a simple scaling analysis of (2.37) and (2.38), for behaviour close to the current's centre, which thus neglects the variation of ϕ with r, and uses $\partial h/\partial r \approx -h_s/r_s$, where subscript s indicates scale, and $\sigma \ll 1$. At the edge, the radial gradient in h and ϕ are large, thus this scaling analysis is not valid there. In this simple model, only two terms remain: the spreading term due to gradients in thickness and the term representing fluid loss

$$\frac{\mathrm{d}h_s}{\mathrm{d}t} = -\frac{\pi}{3V_m}(1 - \beta\phi_s)h_s^5 - (1 - \phi_s)\phi_s^{2-n} \tag{3.1}$$

$$\frac{\mathrm{d}\phi_s}{\mathrm{d}t} = -\frac{(1 - \phi_s)^2 \phi_s^{2-n}}{h_s} \tag{3.2}$$
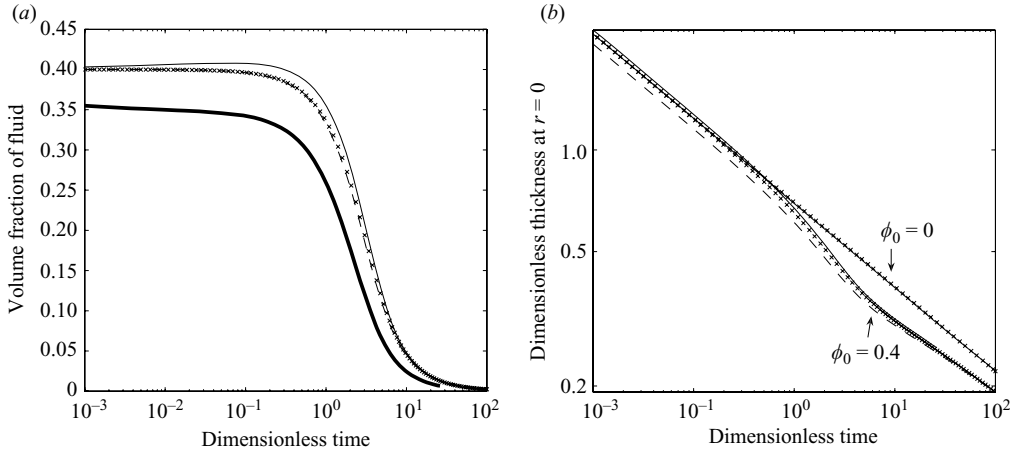
FIGURE 4. Comparison between the numerical calculations and the results given by the simple scaling analysis (3.1) and (3.2) with $\beta = 0.98$ and considering Darcy flow. (*a*) Volume fraction of fluid as a function of time for $\phi_0 = 0.4$. Bold line: average fluid fraction calculated from the numerical model; solid line: fluid fraction at the centre of the current calculated from the numerical model; crosses: fluid fraction calculated from scaling analysis. (*b*) Thickness evolution for $\phi_0 = 0$ and $\phi_0 = 0.4$. Solid lines: thickness calculated from the numerical model; crosses: thickness calculated from scaling analysis. On both graphs, the dashed line indicates the case of $\beta = 0.5$, $\phi_0 = 0.4$, for comparison.

where we have eliminated r_s using $V_m = (1 - \phi_s)\pi h_s r_s^2$, which is the volume of the matrix. The results of this analysis match our more complex calculations, especially for quantities at $r = 0$ (figures 4*a* and 4*b*). Thus, for constant volume, the variation of ϕ over r can be neglected to first order when calculating the average fluid loss and the evolution of the peak thickness.

3.4. *Note on the effect of density and viscosity variations*

The dimensionless number $\beta = \Delta\rho/\rho_m$ does not strongly influence fluid loss but influences the terms of spreading in both the evolution of h and ϕ (see (2.37) and (2.38)). As variations of ϕ with r are negligible far from the edge for constant volume flows, the terms representing spreading due to gradients in fluid volume fraction are negligible in (2.37) and (2.38).

For β close to one, the reduction in spreading rate due to a decrease in density as ϕ increases is counterbalanced by a decrease in viscosity through the factor $(1 - \beta\phi)/(1 - \phi)$ in front of the gradient in thickness in (2.37) and (2.38). For smaller values of β, the effect of viscosity should dominate the spreading behaviour.

Changing β from 0.98 to 0.5, for which the effect of viscosity dominates over density variations, has no effect on fluid loss but changes slightly the evolution in peak thickness with time (figure 4). In the case of $\beta = 0.5$, the mixture density ($\bar{\bar{\rho}} = \rho_m - \phi\Delta\rho$) is larger and spreading is faster. The curve is slightly lower than the curve for $\beta = 0.98$, but this difference diminishes as ϕ decreases and eventually goes to 0 at the end. The effect of different viscosity dependence on ϕ on the spreading of a two-phase gravity currents is examined in Appendix D through the function $\mu_m(1 - \phi)^b$, with $-1 \leqslant b \leqslant 2$. This effect induces very similar changes in the maximum thickness evolution as do variation in β: if the viscosity decreases with ϕ and $b > 1$, the flow spreads more easily, as observed if $\beta = 0.5$, and the peak thickness is smaller at a given time and fluid fraction. If the viscosity increases with

ϕ ($b < 0$), the flow spreads less rapidly and the peak thickness is larger at a given time and fluid fraction; the effect of fluid loss on thickness evolution is even more apparent in that case.

3.5. *Dimensional scaling laws*

3.5.1. *Thickness and radius scales*

The thickness scale for constant volume currents ($Q = 0$), given by (2.34), represents the critical thickness for fluid loss to be significant. In (2.38), when $h \gg 1$, the term representing fluid loss is negligible. The thickness evolution deviates from the single-phase case for $h < 1$ as shown in figures 3(a) and 4(b).

This critical thickness increases with matrix viscosity and current's volume, and decreases with the drag coefficient. The higher the volume and the higher the viscosity, the longer the current remains relatively thick and has time to lose its fluid. A high drag coefficient impedes fluid escape.

Fluid loss is complete when $R \sim 1$ (figure 3b). Thus, the scale R given by (2.36) for $Q = 0$ gives the radius over which fluid loss occurs, which depends mostly on the volume of the current.

3.5.2. *Time scale for complete fluid loss*

Our analysis suggests the rather important result that the time scale for almost complete fluid loss in a constant volume gravity current does not depend on the initial fluid content (figures 2a, b and 4a). This time scale is $\sim 10T$ in the case of Darcy flow, and $\sim 2T$ in the case of suspension flow, with T the time scale given by (2.35), with $Q = 0$ and $c_0 = \mu_f/k_0$ for Darcy flow and $c_0 = 9\mu_m/2r_b^2$ for suspensions. T depends strongly on c_0, and varies only slowly with the volume of the flow and the matrix viscosity.

4. Constant flux gravity currents

In this section, we study flows with a persistent mass source and consider constant volume flux two-phase gravity currents, i.e. $Q > 0$.

4.1. *Thickness and fluid fraction profiles*

The thickness profile and its evolution for the constant flux case is very different from the constant volume case (figure 5a). Current's thickness always increases with time for any given r which leads to a completely different profile for the fluid fraction in the current. In contrast to the constant volume case, we show that the fluid fraction reaches a steady state at the centre, and a significant radial gradient in the fluid fraction develops with time as the current spreads and edge radius increases (figure 5b).

Moreover, in the previous constant volume case, fluid loss is accelerated by the decrease in thickness with time. In the constant flux case, however, as the current spreads and material is injected into it, the thickness at $r = 0$ increases very slightly with time, which inhibits loss of fluid at the centre.

4.2. *Steady-state value of ϕ at the centre*

In the centre of the current, boundary conditions are such that $\partial\phi/\partial r = 0$. In this case, at $r = 0$ (2.38) reduces to

$$\frac{\mathrm{d}\phi}{\mathrm{d}t} = -\frac{(1-\phi)^2\phi^{2-n}}{h} + \frac{1}{\gamma^2}\frac{(\phi_0 - \phi)}{h}. \tag{4.1}$$
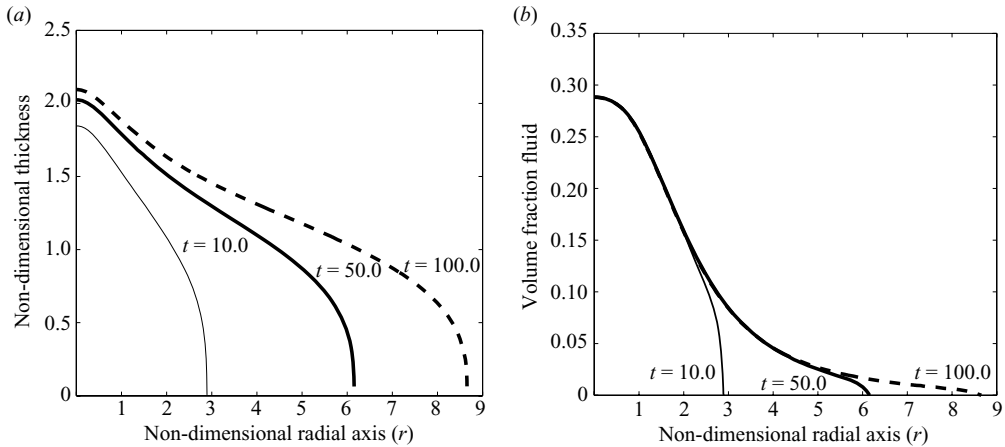
FIGURE 5. (*a*) Thickness h and (*b*) volume fraction of fluid ϕ of a two-phase viscous gravity current as a function of radius r at three different times, for the constant-flux case ($Q > 0$) and considering Darcy flow. Quantities shown are dimensionless. $\phi_0 = 0.3$, $\beta = 0.98$, $\gamma = 0.5$, $V_0 = 1$.
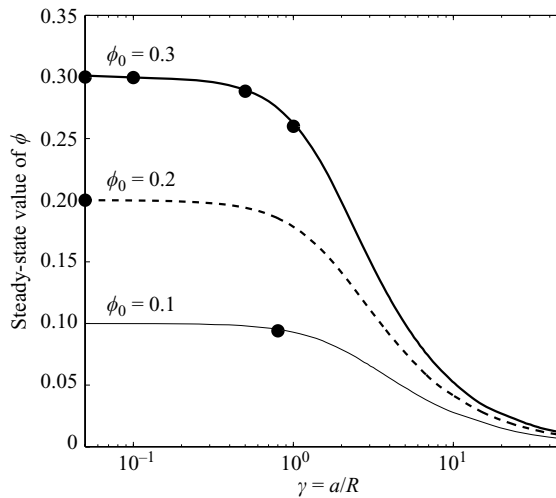

FIGURE 6. Steady-state value of the volume fraction of fluid at the centre of the flow ($r = 0$), considering Darcy flow, as a function of $\gamma = a/R$, and for different values of ϕ_0 indicated on the graphs. Circles: Steady-state value of $\phi(r = 0)$ given by our numerical calculations for different values of ϕ_0 and γ.

At $r = 0$, ϕ attains a steady-state value ϕ_{ss}, when fluid loss is balanced by fluid injection. The steady-state value ϕ_{ss} is the solution to (4.1) for $\mathrm{d}\phi/\mathrm{d}t = 0$, in which case ϕ_{ss} is independent of h and depends only on the initial fluid fraction ϕ_0 and on $\gamma = a/R$. The value of ϕ_{ss} decreases when γ increases, because the source is broader and distributes fluid loss over larger r (figure 6). According to this simple analysis, ϕ_{ss} is significantly less than the initial fraction of fluid ϕ_0 for $\gamma > 1$, i.e. $a > R$. This is generally not relevant for geological flows, for instance volcanic conduits are much smaller than the characteristic radius R of a lava flow ($\gamma < 1$).
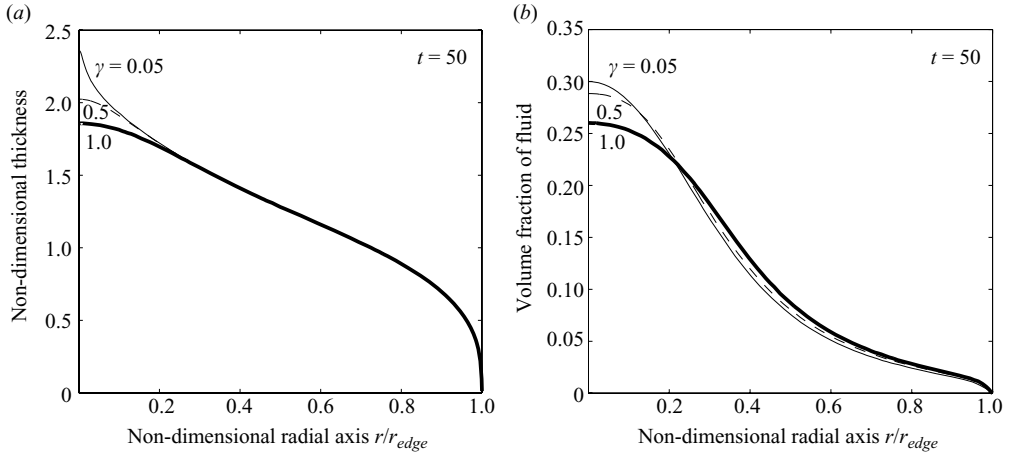
(a)

(b)

FIGURE 7. (*a*) Thickness and (*b*) volume fraction of fluid as a function of radial direction r normalized by edge radius, at $t = 50$, for different values of γ indicated on the graph, for the constant flux case ($Q > 0$) and considering Darcy flow. Parameters are dimensionless. $\phi_0 = 0.3$, $\beta = 0.98$, $\sigma \ll 1$, $\nu \ll 1$, $V_0 = 1$.

Steady-state values of ϕ at $r = 0$ derived from our numerical calculations for Darcy flow and for different values of ϕ_0 and γ, match the theoretical results given by (4.1) for $\mathrm{d}\phi/\mathrm{d}t = 0$ (figure 6).

In numerical calculations, steady-state values of ϕ are reached when the dimensionless edge radius of the current attains about three times the value of the dimensionless radius of the source γ. After this initial period, γ has only little influence on the results.

4.3. *Effect of* γ

As demonstrated by the scaling analysis, decreasing the size of the source γ causes the centre of the current to become thicker and to retain a larger steady-state fluid fraction (figure 7*a*, *b*). As the typical radius of the source γ decreases, both the thickness and fluid fraction develop higher gradients far from the front. However, the average fluid fractions in the current are very similar for different values of γ (for a given time t and initial fluid fraction ϕ_0), and hence the size of the source has a negligible influence on fluid loss.

4.4. *Fluid fraction evolution*

Because ϕ reaches a steady state at the current centre, the fluid fraction profile as a function of radius remains identical through time near $r = 0$ (figure 5*b*). The fraction of fluid stays significant in the range $0 \leqslant r \leqslant 6$ and becomes negligible once the edge radius exceeds $r = 10$. Significant fluid loss occurs then between $r = 0$ and $r \sim 8$ for Darcy flow. The dimensional radial scale over which fluid loss occurs is approximately $8R$ for Darcy flow; it is equal to $2R$ for a suspension flow. Once the radius of the flow exceeds this radial scale, the fluid fraction profile remains similar.

The evolution of the average fluid fraction $\langle \phi \rangle$ depends only on the initial volume fraction of fluid ϕ_0, as in the case of the constant volume flow. As in the constant volume case, fluid loss becomes significant for $t > 1$ for Darcy flow (figure 8*a*), at which time $r \sim 1$, and the higher the initial fluid fraction, the higher the rate of fluid loss.
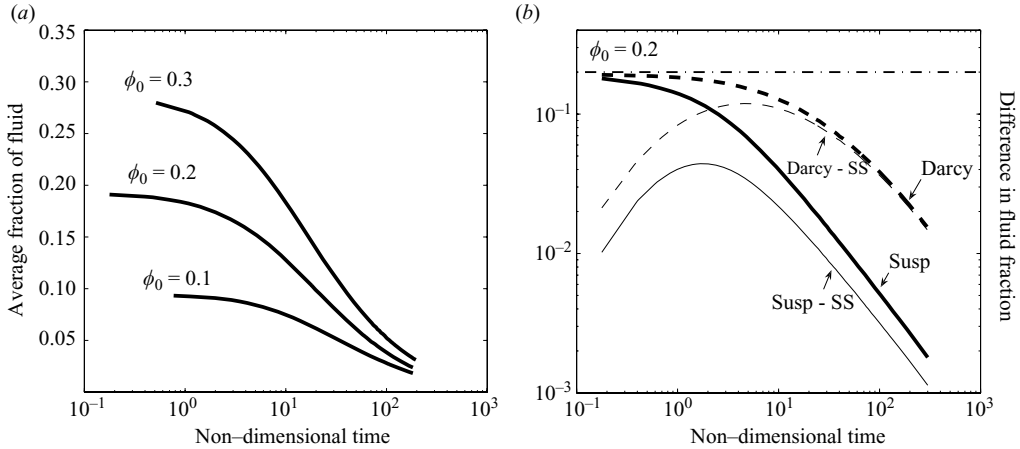
FIGURE 8. Average fraction of fluid in the current $\langle\phi\rangle$ as a function of dimensionless time, in the case of constant flux flows ($Q > 0$), using $V_0 = 1$, $\beta = 0.98$, $\sigma \ll 1$, $\nu \ll 1$. (*a*) Evolution for different values of $\phi_0 = 0.3$, 0.2 and 0.1, and considering Darcy flow. (*b*) Evolution for $\phi_0 = 0.2$ considering a suspension flow (thick solid line), and Darcy flow (thick dashed line). Note the scale change from linear (*a*) to logarithmic (*b*) in the vertical axis. The dash-dotted line indicates the limiting case of no fluid loss, i.e. constant fluid fraction with time. Thin lines correspond to the difference in fluid fraction between a two-phase compacting gravity–current and a theoretical 'steady-state' case. In the limiting steady-state case, the initial volume is $V_0 = 1$ with $\phi_0 = 0.2$ and all the fluid subsequently injected is lost at the surface. Thin line: difference between suspension flow and steady-state case; thin dashed line: difference between Darcy flow (dashed line) and steady-state case.

The volume-averaged fluid fraction $\langle\phi\rangle$ decreases with time, as the total volume increases and fluid is lost at the surface (figure 8*a*). For Darcy flow, fluid loss becomes significant at $t > 1$, $r > 1$, and at $t = 200$ the volume fraction of fluid reaches 10 % of the initial fraction of fluid ϕ_0, for any value of ϕ_0. However, fluid loss still continues after this time because of new injection, but the volume of fluid remaining in the current becomes negligible in comparison to the total volume.

One can compare the evolution of the average fluid fraction with two limiting cases. In the first limit, there is no loss of fluid, and the amount of fluid remains constant in the current. In the second limit, corresponding to a steady state, the current starts with a volume $V_0 = 1$ containing a fraction of fluid $\phi_0 = 0.2$, and all the subsequent fluid injected is lost at the surface, which leads to $\langle\phi\rangle = \phi_0 V_0/(V_0 + Qt)$. The difference in fluid fraction between the calculated gravity currents and this hypothetical steady-state case initially increases, because the flow retains fluid (figure 8*b*) and then decreases when the flow approaches steady-state fluid loss (figure 8*b*). We define the characteristic time for fluid loss to reach steady state as the time for this difference to reach 10 % of the initial fluid fraction (i.e. 0.02 in the case of figure 8*b*).

For Darcy flow, it takes $\sim 200T$ to reach a steady-state evolution at which time the current's radius is $12.7R$, with T and R the characteristic time scale and radius scale, respectively, given by (2.35) and (2.36), with $Q > 0$ and $c_0 = \mu_f/k_0$. For a suspension flow, it takes $10T$ to reach steady-state conditions, at which time the current's radius is $2.9R$, with T and R, respectively, given by (2.35) and (2.36), with $Q > 0$ and $c_0 = 9\mu_m/2r_b^2$. This compares favourably with the 'fluid loss radii' of $\sim 8R$ and $\sim 2R$ discussed above.

5. Application to the spreading and degassing of lava flows

Here we apply the results of our modelling to study the coupling between the spreading and degassing of a lava flow. The validity of the assumptions used in the model are first verified for the case of lava flows; and we infer a range of values for model parameters and dimensionless numbers.

5.1. *Assumptions and parameters*

5.1.1. *Viscosity and density*

The application to lava flows requires $\mu_f \ll \mu_m$ and $\rho_f < \rho_m$, where the fluid phase is the gas. Gas viscosity μ_f is about 10^{-5} Pa s for H_2O and CO_2 gas. Lava viscosity depends on its composition, silica and water content in particular; it can vary between 10 Pa s for mafic lavas and more than 10^8 Pa s for felsic lavas. The effective viscosity based on simple mixture theory goes as $\mu_m(1 - \phi)$. However, the behaviour of lava flows may be more complex (Llewellin, Mader & Wilson 2002), but different dependences of the viscosity on gas volume fraction have little effect on the degassing process and only affect the shape of the flow (see Appendix D).

Lava density ρ_m depends mainly on its composition and varies between ∼2300 kg m^{-3}, for felsic lavas, and ∼3000 kg m^{-3}, for mafic lavas.

Gas density ρ_f is 0.59 and 1.98 kg m^{-3} for water vapour and carbon dioxide, respectively, at 1 atm and 373 K. Gases are compressible and their densities vary with temperature and pressure. However, in lava flows, temperature variations are limited to flow margins; the effect of pressure may be more important. Following the ideal gas law, one can estimate that gas density increases from ∼0.59 kg m^{-3} at the top to ∼38 kg m^{-3} at the bottom of a 100 m thick magma column, i.e. $\Delta\rho/\rho_m$ varies between 0.9998 and 0.9848, using $\rho_m = 2500$ kg m^{-3}. Therefore this variation can be neglected and $\beta = \Delta\rho/\rho_m$ can be considered constant, between 0.98 and 1 as calculated above.

5.1.2. *Values of $\sigma = H^2/R^2$*

In the case of very fluid lavas, such as basalts, or when the porosity becomes very low, the gas phase forms isolated bubbles which are treated as suspensions. In that case $c_0 = 9\mu_m/2r_b^2$ (Appendix A). For bubble radii r_b between 0.1 and 10 mm, and lava viscosities between 10 and 10^4 Pa s, the range of values for c_0 is 4.5×10^5 to 4.5×10^{12} Pa s m^{-2}. In that case we always have $\sigma \ll 1$, even for large bubble radius and small volume or volume flux lava flows (see (2.42)).

In the case of large viscosity lavas, such as andesites, dacites or rhyolites, which contain microcrystals and a high proportion of gas, the gas may form a complex and interconnected network. The interaction force follows Darcy's law and the drag coefficient is such that $c = \mu_f/k_0$ is a constant, $n = 0$ in (2.29) and (2.30) (see Appendix A). For porosity between 30 % and 60 %, permeability varies over several orders of magnitude, with values between 10^{-16} and 10^{-12} m^2 for felsic samples (Eichelberger *et al.* 1986; Klug & Cashman 1996). Using $k(\varphi) = k_0\varphi^2$, k_0 is between 10^{-12} and 10^{-15} m^2, which gives a range of values for c_0 between 10^7 and 10^{10} Pa s m^{-2}. Emplacement of lava domes are eruptions characterized by large viscosities and small flux or volumes, of the order of 1 m^3 s^{-1} and 10^8 m^3, respectively, for the well-known examples of the Mount St Helens and the Soufrière Hills (Montserrat) domes (Sparks *et al.* 1998), and hence largest values of σ (see (2.42)). Using $V_0 \geqslant 10^6$ m^3 and $Q = 1$ m^3 s^{-1} and a large value of $\mu_m = 10^8$ Pa s, we find that σ is less than 0.025 and 0.3 in the constant volume and constant flux case, respectively.

To summarize, in the vast majority of cases: $\sigma \ll 1$, and thus $\nu \ll 1$, and the terms involving horizontal phase separation and compaction are negligible in (2.37) and (2.38), as considered in our calculations (§§ 3 and 4).

5.2. *Two volcanic examples*

5.2.1. *Degassing of a felsic lava dome*

In felsic volcanic systems, the gas phase may form an interconnected network, in which case we use $c_0 = \mu_f/k_0 = 10^9$ Pa s m^{-2} and $n = 0$, $\mu_m = 10^8$ Pa s, $\rho_m = 2500$ kg m^{-3}, $\beta = 0.98$ and $g = 9.81$ m s^{-2}. We consider an average flux of $Q = 1$ m^3 s^{-1}, a typical value for effusion rates measured on various domes (Sparks *et al.* 1998; Nakada & Motomura 1999). According to our calculations, significant degassing occurs over a radius of $\sim 8R$, i.e. over ~ 900 m. The flow retains gas and returns to a steady state where all the injected gas is lost by degassing, in $\sim 200T = 1.6$ year, with T given by (2.35) for $Q > 0$. This time period is comparable to the typical duration of dome growth. Domes contain a significant fraction of gas; for instance, measurements in an obsidian dome of the Inyo Domes chain, California, show porosities between 15 % and 30 % (Eichelberger *et al.* 1986). Degassing is thus likely to influence the spreading of the dome and, for a given effusion rate, to decrease the advance rate of the flow front and the average growth rate in comparison to a single-phase lava flow (figure 3*a*, *b*). Thus degassing might in part account for the slow decrease in the growth rate and the advance rate of the flow front noted by Huppert *et al.* (1982) at La Soufrière Saint Vincent, which was attributed to the growth of a rubble collar at the front. This decrease in both rates happened after 70 days of dome growth, at an average growth rate of 6 m^3 s^{-1}, at which time the thickness and radius, respectively, reached ~ 120 and ~ 400 m. In our results, degassing becomes significant when the dimensionless time and radius are both ~ 1. For relevant values of the viscosity and of the reference permeability of 3×10^{11} Pa s and 5×10^{-15} m^2, such that degassing starts at $t \sim T = 70$ days, the radius is $R \sim 400$ m and the thickness at the centre for a conduit radius $a \sim 20$ m is $2H \sim 140$ m, close to the values measured at the Soufrière Saint Vincent after an equivalent time interval.

5.2.2. *Flood basalt lava flows*

In analogy to active inflated pahoehoe flows observed in Hawaii, Self, Keszthelyi & Thordarson (1998) suggested that flood basalts may be emplaced as large inflated flow fields, involving the raising of the upper crust of a lava flow as fresh lava is injected into the molten core of the flow. Our degassing model may not be significantly affected by a mechanism of inflation, as long as the crust is weak and deformable. A weak crust acts only as an insulator, supporting our assumption of an isothermal flow, and does not mechanically influence the spreading of the lava. Degassing would be slowed down only if the crust has a lower permeability than the lava. But, while the crust is inflated by a lava flow, it is deformed and fractured and hence permeable. However, if the crust is thick and hardly deformable, it influences the dynamics of the flow, which is then similar to the spreading of a laccolith in an elastic media (Johnson & Pollard 1973). The elastic response of the crust will accelerate the spreading of the flow by squeezing the lava outwards, and our model then provides a lower limit for the radial extent of the degassing.

We thus use the results of our model to estimate the extent of degassing of flood basalt flows. In basaltic flows, gas bubbles form a suspension; the reference drag coefficient is defined by $c_0 = 9\mu_m/2r_b^2$ and takes values between 5×10^9 and

5×10^{11} Pa s m^{-2}, for lava viscosity between $\sim 10^2$ and 10^3 Pa s, and gas bubble radii between 0.1 and 1 mm. We use $\rho_m = 2800$ kg m^{-3}, $g = 9.81$ m s^{-1} and $\beta = 0.98$.

Self *et al.* (2006) estimated volumes and effusion rates for Columbia River flood basalt flows of ~ 1000 km^3 and ~ 4000 m^3 s^{-1}, respectively.

For those typical volumes and effusion rates, we calculate that degassing of a flood basalt flow occurs over a radius equal to $R = 200$–400 km, for a typical volume of 1000 km^3, with R given by (2.36) for $Q = 0$, or over a radius equal to $2R = 30$–300 km for a volume flux equal to 4000 m^3 s^{-1}, with R given by (2.36), depending on the drag coefficient. Thus, results from constant flux and volume are consistent with each other and indicate that the surface area over which significant degassing occurs could reach more than 10^5 km^2.

This result shows that gas is retained within the lava and transported over large distances. Although we do not consider cooling in our model, one can reasonably assume that gas released near the vent will be at a higher temperature than gas released far from the vent. Initial explosive eruptions of volatile-rich basalts release hot gas at the vent that may reach the stratosphere (Thordarson & Self 1993). In contrast, subsequent effusive eruptions distribute cooler gas over a large area, which may affect vertical gas transport. For example, according to our model, the radius over which gas is released reaches a few hundreds of kilometres and can approach the Rossby radius of deformation $R_{rd} = \sqrt{gH'\Delta T/T_0}/(2\Omega \sin\alpha)$ (Gill 1982), where α is the latitude, H' is the characteristic height of the flow of gas in the atmosphere, $g = 9.81$ m s^{-2} is the acceleration of gravity and $\Omega = 7.2 \times 10^{-5}$ rad s^{-1} is the Earth's angular velocity. H' is approximately 100 m and for $\Delta T/T_0 \approx 200/300$, we find that at latitudes larger than or equal to $\sim 35°$, the Rossby radius of deformation is less than 300 km and gas released into the atmosphere by flood basalt lava flows may become sensitive to the Earth's rotation and undergo cyclonic activity.

5.2.3. *Effect of cooling and phase changes*

Gas exsolution may generate secondary populations of gas bubbles, which in turn would affect the spreading of the flow. As the flow thins, exsolution takes place, in particular at the base of the flow, where the pressure decreases significantly. This would lead to a change in viscosity and volume of the mixture through the change in gas volume fraction, which would in part compensate for gas loss. But, it would also lead to a significant increase in the melt (matrix) viscosity, as the melt becomes drier. This effect could be significant in the case of thick felsic lava domes, as they contain a significant fraction of dissolved volatiles that largely affect their viscosity. Although the present model does not include gas exsolution it can be readily added.

Cooling and solidification of the lava, which are not taken into account in this theory, might also influence the spreading and degassing of the flow and necessitate a more complex theory. However, some conclusions can be derived by comparing the time scales for degassing to the time scale for cooling and solidification of a particular lava flow. Time scale for cooling by radiation and emplacement of single-lobed basaltic flows are, for instance, given by Crisp & Baloga (1990).

Time scales for the solidification of a lava flow surface are also given by Fink & Griffiths (1990) and Griffiths & Fink (1992) and are between a few tens to a few hundreds of seconds and are thus much smaller than the time scale for degassing as estimated by our study. As discussed in the previous section, however, the presence of a crust does not necessarily influence the rise of the gas phase within the flow, since the passage of gas through the crust is achieved rapidly through fractures.

6. Conclusion

We have developed a theory for the evolution of the thickness and fluid fraction of a two-phase viscous gravity current composed of a viscous matrix and much less viscous fluid. Loss of fluid is accounted for by flux through the upper boundary. The resulting theory is valid both for the case of a suspension of fluid particles within the matrix, and for the case of Darcy flow through a permeable matrix; in the latter case the compaction length is assumed less than the thickness of the flow. Scaling analysis shows that the horizontal separation of phases may be neglected in most natural settings. Numerical analysis of the governing equations, for both constant volume and constant volume–flux flows, shows that rate of fluid loss is only a function of the initial fluid fraction, but occurs in a finite radius and within a finite time scale. The fluid-loss radius and time scale, however, are independent of initial fluid fraction, but are functions of the physical properties of the two phases, as well as the volume or flux of the flow. Fluid loss affects the rate of spreading of the current (i.e. evolution of the thickness and radius as a function of time) relative to a single-phase gravity current. Moreover, the effective mixture viscosity's dependence on fluid fraction can change the current's shape. The application to lava flow shows that volcanic gas (acting as the fluid phase) is retained over a large extent. Degassing can therefore change the rate of spreading of a dome. In the case of flood basalt lava flows, the distances over which degassing occurs might reach length scales at which the ascent of gas in the atmosphere becomes sensitive to the Coriolis effect, thereby causing cyclonic activity and affecting atmosphere dynamics.

Appendix A. Drag coefficient for suspensions and Darcy flow

The drag coefficient c controls the viscous interaction between phases and is one of the critical parameters of our model since it plays an important role in the characteristic values of thickness H and time scale T.

If the fluid forms an interconnected network, the interaction force follows Darcy's law and the drag coefficient depends on the fluid viscosity and on the size of matrix pores which controls its permeability (McKenzie 1984). Bercovici *et al.* (2001*a*) show that, for $\mu_f \ll \mu_m$, $c = \mu_f \varphi^2 / k(\varphi)$, where $k(\varphi)$ is the permeability which depends on the porosity or fluid fraction φ. For small porosities, one often uses the simple model $k(\varphi) = k_0 \varphi^n$ (e.g. see Spiegelman 1993*c*). We use $n = 2$, which gives $c = \mu_f / k_0 = c_0$ constant (i.e. $c = c_0 \varphi^n$, $n = 0$), representative of tubules for fluid transport.

The fluid phase may also form isolated particles or bubbles, which can be treated as a suspension; this is the case for gas bubbles in basaltic lavas (Manga 1996). The interaction force between phases follows Stoke's law. For one particle of radius r_b and density ρ_f in matrix, the velocity difference between the particle and matrix is given by

$$0 = \frac{4\pi}{3} r_b^3 (\rho_f - \rho_m) g \mathbf{z} - 6\pi \mu_m r_b \Delta \mathbf{v} \qquad (A\,1)$$

which is appropriate for stokeslet with free slip surfaces. For N particles in a volume δV_T, with $\varphi = N 4\pi r_b^3 / 3 \delta V_T$ and accounting for Archimedean compensation of the

other bubbles, we have

$$0 = N\frac{4\pi}{3}r_b^3(\rho_f - (1-\varphi)\rho_m - \varphi\rho_f)gz - 6N\pi\mu_m r_b \Delta v \quad (A\,2)$$

which gives

$$0 = -\varphi(1-\varphi)\Delta\rho gz - \varphi\frac{9\mu_m}{2r_b^2}\Delta v \quad (A\,3)$$

By analogy with the action–reaction equation (2.7), with $\Delta P = 0$, $\tau = 0$ and $\nabla\phi = 0$, we obtain

$$c = \varphi\frac{9\mu_m}{2r_b^2}. \quad (A\,4)$$

If we consider that particle radius remains constant when φ varies and only the number of particles N varies, then $c = c_0\varphi^n$ with $n = 1$ and $c_0 = 9\mu_m/2r_b^2$.

Appendix B. Effects of viscous compaction

Here we examine the effects of viscous compaction and a finite pressure difference between phases ΔP on fluid loss, which occur primarily through the vertical rate of phase separation at the surface, $\Delta w(z = h)$. We verify in particular that ΔP is indeed negligible and that viscous compaction has little or no effects on fluid loss for $\sigma \ll 1$, as is relevant for most geologic flows (e.g. lavas). We start from (2.12), with $\theta \ll \varphi$, i.e. $\varphi \sim \phi$. The exact solution of this equation is

$$\frac{\partial P_f}{\partial z} = A_1 e^{r_1 z} + A_2 e^{r_2 z} - \left(\bar{\rho}g + 2\frac{\theta^2}{h^2}\delta^2\rho_f g\right)\left(1 + 2\frac{\theta^2}{h^2}\delta^2\right)^{-1}, \quad (B\,1)$$

where A_1 and A_2 are two constants of integration, and r_1 and r_2 are given by

$$r_{1,2} = \frac{\theta}{h}\left[-(3-4\phi) \pm \left((3-4\phi)^2 + 4\phi(1-\phi)\left(\frac{h^2}{\theta^2\delta^2}+2\right)\right)^{1/2}\right](2\phi(1-\phi))^{-1}. \quad (B\,2)$$

Thus Δw and ΔP are determined by using (B 1) in (2.4) and (2.11), respectively. A_1 and A_2 are determined by the following boundary conditions. At $z = 0$, the boundary is rigid and impermeable and there is no relative vertical motion between fluid and matrix, $\Delta w = 0$. Note that we also consider a flux of mixture feeding the current at a given constant volume rate Q through the lower boundary, but in that case also, both phases are injected at the same velocity and $\Delta w = 0$. At $z = h$, we consider $\Delta P = 0$, since $P_f = P_m = P_a$ when $\mu_m W/H$ is negligible relative to P_m (see discussion in §2.2.2 about the stress tensor components). This is consistent with the fact that ΔP should decrease with height because the difference in mass between columns of matrix and fluid decreases.

We have therefore

$$\Delta P = \frac{(1-\phi)\delta^2/h}{1 + 2\delta^2\theta^2/h^2}\Delta\rho g \times [2\theta - B_1(2\theta + r_1 h\phi)e^{r_1 z} - B_2(2\theta + r_2 h\phi)e^{r_2 z}] \quad (B\,3)$$

$$\Delta w = -\frac{\Delta\rho g}{c_0}\frac{(1-\phi)\phi}{1 + 2\delta^2\theta^2/h^2} \times [(1-\phi) - B_1 e^{r_1 z} - B_2 e^{r_2 z}], \quad (B\,4)$$
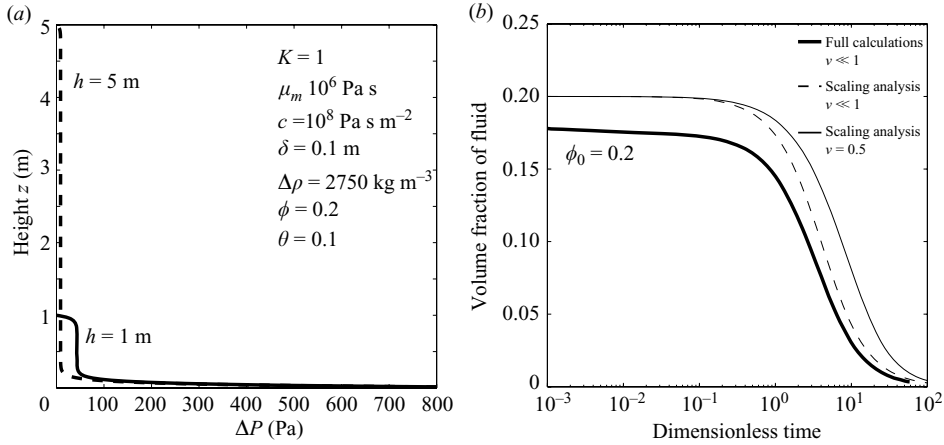
FIGURE 9. (*a*) Two profiles for the value of ΔP as a function of z given by (B 3) for two different values of $h = 5$ and 1 m. Values of the other parameters are given on the graph. (*b*) Evolution of the average fluid fraction $\langle \phi \rangle$ as a function of time, for $\phi_0 = 0.2$ and for two different cases: $\nu \ll 1$ and $\nu = 0.5$, Δw is given by (B 4). The results of the full calculations for the case $\nu \ll 1$ are also shown for comparison.

where B_1 and B_2 are both positive

$$B_2 = (2\theta - (2\theta + r_1 h\phi)e^{r_1 h}) \times ((2\theta + r_2 h\phi)e^{r_2 h} - (2\theta + r_1 h\phi)e^{r_1 h})^{-1} \quad \text{(B 5)}$$

$$B_1 = 1 - B_2. \quad \text{(B 6)}$$

We take the example of a lava flow and parameters are chosen such that the compaction length is not too small: $\mu_m = 10^6$ Pa s, $c_0 = 10^8$ Pa s m^{-2}, $\delta = (K\mu_m/c_0)^{1/2} = 0.1$ m. For such a high viscosity, the characteristic thickness H of the flow, given by (2.34) for $Q = 0$ is of 1.25 m for a 1000 m^3 lava flows and of several metres for more relevant higher volumes. It is thus much larger than the compaction length, which supports our assumption that $\delta^2 \ll H^2$, i.e. $\nu^2 \ll 1$.

We choose the thickness h such that it is close to the characteristic thickness H and we calculate that ΔP at $z = 0$ is equal to 1085 Pa, for $h = 5$ m and 1109 Pa for $h = 1$ m. These values for ΔP are negligible in comparison with $\bar{\rho}gh$ equal to 2.2×10^4 and 1.1×10^5 Pa for $\phi = 0.2$ and $h = 1$ and 5 m, respectively. With increasing z, the pressure difference drops within roughly one compaction length to a value of 8.6 Pa, for $h = 5$ m , and 43.2 Pa, for $h = 1$ m, and stays constant over most of the flow height (figure 9a).

For comparison, ΔP estimated from (2.19) is 7.6 Pa for $h = 5$ m and 37.8 Pa for $h = 1$ m, which is close to the values calculated with (B 3) over the major height of the flow. ΔP increases when the ratio δ/h decreases but is negligible for $\delta/h \leqslant 0.1$.

When $\delta/h \leqslant 0.1$ then r_1 and r_2 reduce to much simpler forms

$$r_1 \sim -\frac{1}{d} \quad \text{(B 7)}$$

$$r_2 \sim +\frac{1}{d} \quad \text{(B 8)}$$

with $d = \delta((1 - \varphi)\varphi)^{1/2}$. We have then

$$B_2 \sim \frac{2\theta - e^{-h/d}(2\theta - \phi h/d)}{e^{h/d}(2\theta + \phi h/d)} \tag{B 9}$$

$$B_1 = 1 - B_2 \simeq 1 \tag{B 10}$$

At $z = h$, we have, for d small relative to h

$$\Delta w(h) = -\frac{\Delta \rho g}{c_0} \phi(1 - \phi) \times \left[-1 + e^{-h/d} - \frac{2\theta - e^{-h/d}(2\theta - \phi h/d)}{2\theta + \phi h/d} \right] \tag{B 11}$$

$$\Rightarrow \Delta w(h) \simeq -\frac{\Delta \rho g}{c_0} \phi(1 - \phi) \tag{B 12}$$

which validates our assumptions and confirms (2.28). At $z = h$, well above the compactive boundary layer at the bottom of the flow, the difference in velocity ceases to be a function of z.

Equation (B 4) shows however, that, for larger δ/h, as B_1 and B_2 are positive, compaction would reduce the difference in velocity at the surface of the flow, and thus reduce the rate of fluid loss. For larger δ/h, matrix resistance to deformation would be the limiting process for fluid loss.

Using the simple scaling analysis of §3.3 for constant volume flows, we calculate the effect of matrix resistance to compaction on fluid loss for $\nu = \delta/H = 0.5$. In that case we can still consider ν^2 and σ small and ΔP is still negligible relative to P_f. Compaction affects only the terms involving Δw, i.e. fluid loss at the surface, in (2.29) and (2.30). We use (B 4) for the expression for Δw and $\theta = \phi/2$ to calculate the rate of fluid loss in (3.1) and (3.2).

Matrix resistance to compaction plays a role when ν is no longer negligible (figure 9b). When ν is closer to unity, resistance to compaction limits the loss of fluid and causes a decrease in the rate of fluid loss as predicted earlier.

Appendix C. Numerical resolution

The governing equations for the two-phase gravity current (2.37) and (2.38) are solved numerically with finite volumes (Patankar 1980). The last grid point included in the calculations occurs at grid point $i = i_{max}$, which varies as the current spreads and the edge increases. This edge point is calculated for each iteration such that $h_{i=i_{max}} > 0$ and $h_{i>i_{max}} = 0$, so that both h and ϕ are defined on all the grid points used in the calculations. This method leads to the inversion of a tridiagonal matrix for both h_i^{n+1} and ϕ_i^{n+1}, at time step $n + 1$. The inversion is realized from $i = i_{max}$ to $i = 1$. At $r = 0$, $\partial h/\partial r = 0$ and $\partial \phi/\partial r = 0$, which gives $h_{i=1} = h_{i=2}$ and $\phi_{i=1} = \phi_{i=2}$.

The advective terms proportional to $\partial \phi/\partial r$ in (2.38) need careful treatment. A centred-difference scheme, consistent with the finite-volume method, is unstable; we replace it with an upwind difference scheme and write it as $(\partial \phi/\partial r)_i = 0.8(\phi_{i+1} - \phi_{i-1})/2\Delta r + 0.2(\phi_i - \phi_{i-1})/\Delta r$, but still use $(\partial h/\partial r)_i = (h_{i+1} - h_{i-1})/2\Delta r$. To mitigate the instability coming from the relaxation of the initially imposed fluid fraction profile, the term $\phi_i(t)$ used to calculate the time derivative $(\partial \phi/\partial t)_i = (\phi_i(t + \Delta t) - \phi_i(t))/\Delta t$ is averaged over three grid points: $\phi_i(t) = a\phi_{i-1}(t) + (1 - 2a)\phi_i(t) + a\phi_{i+1}(t)$. We use the smallest possible value for a: $a = 5 \times 10^{-4}$, which gives the same results as $a = 10^{-3}$.

Equations (2.37) and (2.38) have typical advection and diffusion terms. We use CFL conditions to determine the value of the optimal time step (Courant, Friedrichs & Lewy 1967).

Appendix D. Variations in viscosity with fluid volume fraction

Here, we examine the effect of different viscosity variations with fluid fraction. To be consistent with the simple two-phase mixture theory, we assume in the main text that the current viscosity varies as $\mu_m(1-\phi)$. But this linear viscosity variation with fluid fraction is not always realistic. Viscosity of a mixture may be nonlinearly dependent on ϕ and may even increase with the fluid fraction; this may be the case for flows with suspended gas bubbles, depending on the effective bubble rigidity (Llewellin *et al.* 2002). If the bubbles deform easily and the surface tension is low, then viscosity decreases as ϕ increases.

In order to examine the effect of more complex rheologies, we have used the following effective viscosity for the flow: $\mu_{eff} = \mu_m(1-\phi)^b$, which allows a direct comparison with the general two-phase theory for $b = 1$. For $b > 0$, viscosity decreases with increasing fluid fraction. In the case where $b < 0$, the viscosity increases with the fluid fraction, which is relevant for a 'rigid' suspension of gas bubbles. Using the new function for the mixture viscosity, the equations for the evolution of thickness and fluid fraction become

$$\frac{\partial h}{\partial t} = \frac{1}{r}\frac{\partial}{\partial r}\left[\frac{(1-\beta\phi)h^3 r}{3(1-\phi)^b}\frac{\partial h}{\partial r} - \frac{\beta h^4 r}{8(1-\phi)^b}\frac{\partial \phi}{\partial r}\right]$$

$$+\frac{\sigma}{r}\frac{\partial}{\partial r}\left[\frac{(1-\beta\phi)}{\beta}\phi^{2-n}hr\frac{\partial h}{\partial r} - \frac{\phi^{2-n}h^2 r}{2}\frac{\partial \phi}{\partial r}\right]$$

$$+\frac{1}{\gamma^2}e^{-r^2/\gamma^2} - \phi^{2-n}\left[(1-\phi) - \sigma\frac{(1-\beta\phi)}{\beta}\left(\frac{\partial h}{\partial r}\right)^2\right] \tag{D 1}$$

$$\frac{\partial \phi}{\partial t} = \frac{\partial \phi}{\partial r}\left[\frac{(1-\beta\phi)h^2}{3(1-\phi)^b}\frac{\partial h}{\partial r} - \frac{\beta h^3}{8(1-\phi)^b}\frac{\partial \phi}{\partial r}\right]$$

$$+\sigma\frac{(1-\phi)}{rh}\frac{\partial}{\partial r}\left[\frac{(1-\beta\phi)}{\beta}\phi^{2-n}hr\frac{\partial h}{\partial r} - \frac{\phi^{2-n}h^2 r}{2}\frac{\partial \phi}{\partial r}\right]$$

$$+\frac{(\phi_0 - \phi)}{h}\frac{1}{\gamma^2}e^{-r^2/\gamma^2} - \frac{(1-\phi)\phi^{2-n}}{h}\left[(1-\phi) - \sigma\frac{(1-\beta\phi)}{\beta}\left(\frac{\partial h}{\partial r}\right)^2\right]. \tag{D 2}$$

The shape of a two-phase gravity current differs for different values of the exponent b (figure 10a), although the radial profile of the fluid fraction does not change. For $b = 1$ the shape is similar to a single-phase gravity current. For $b > 1$, the viscosity decreases even more with fluid fraction, and the current spreads more readily for a higher fraction of fluid, thus the current is flatter at the centre, where ϕ is higher and it spreads more easily with less pressure gradient. The fluid fraction decreases significantly closer to the front and the viscosity increases rapidly, leading to a more abrupt front similar to the behaviour of cooling gravity currents (Stasiuk *et al.* 1993; Bercovici & Lin 1996). For $b < 0$, the viscosity increases away from the front, which leads to a less abrupt front, and a more gradual slope to the current.

As b increases, the viscosity decreases for a given fluid fraction, thus the current surface area increases with b at a given time and ϕ_0. This should facilitate fluid loss, but, in fact, this effect is negligible and leads to a difference of less than 0.5 % in fluid fraction at a given time for an increase of b from 1 to 2. Fluid loss as a function of time cannot be differentiated from that shown in figure 2. The effect is more significant on the evolution of thickness and edge radius, although the general
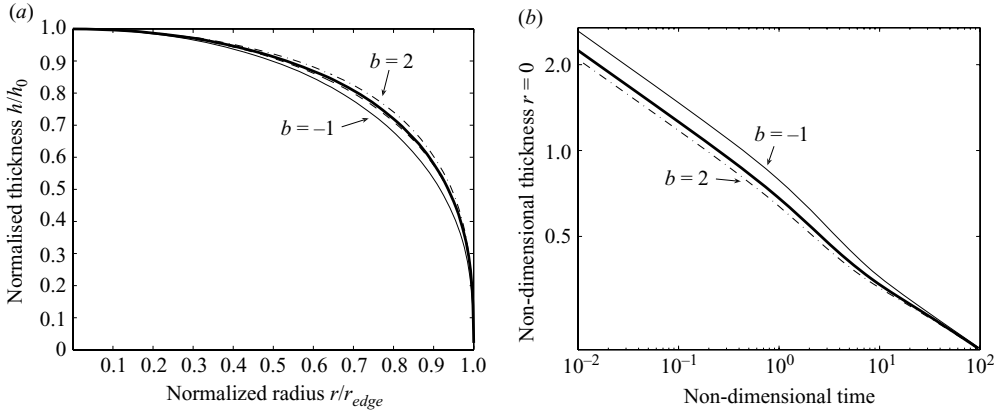
FIGURE 10. (*a*) Comparison of the shape of two-phase viscous gravity currents as the current loses its fluid phase, for different values of the exponent *b*, for Darcy flow. Also indicated on the graph in dashed line is the self-similar shape of a single-phase gravity current. For $b = 1$, the shape is very similar to a single-phase gravity current. (*b*) Evolution of the thickness as a function of dimensionless time, for different values of the exponent *b*, for Darcy flow. Effective viscosity varies with the fluid fraction as $\mu_m (1 - \phi)^b$. Bold line: $b = 1$, viscosity decreases linearly with fluid fraction; dash-dotted line: $b = 2$, viscosity decreases even more with fluid fraction; solid line: $b = -1$, viscosity increases with fluid fraction.

behaviour does not change. As *b* decreases, the viscosity is higher for a given fluid fraction, the current spreads less easily and remains thick for longer times (figure 10*b*). The effect of fluid loss on the current's thickness evolution becomes more evident as *b* decreases. As ϕ goes to 0, the thickness (and edge radius) evolution returns to the single-phase evolution.

Appendix E. Effect of finite vertical variations of φ

Here we study the effect of large variation of φ over height *z*. We consider that $\nu \ll 1$ and $\sigma \ll 1$, i.e. the terms coming from compaction and horizontal separation of fluid and matrix are negligible, and we consider Darcy flow such that $c = c_0 = \mu_f / k_0$ and $n = 0$. Variations of φ are assumed linear over *z*, i.e. $\varphi(z) = 2\theta z / h$ and we consider small values of φ such that $(1 - \varphi)^{-1} \sim 1 + \varphi$. The dimensionless equations for the evolution of θ and *h* over *t* gives then, with $\partial_r = \partial / \partial_r$

$$\frac{\partial h}{\partial t} = \frac{1}{3r} \partial_r ((1 + \theta/2) r h^3 \partial_r h) - \frac{\beta}{r} \partial_r \left(\left(\frac{29}{60} + \frac{23}{90} \theta \right) \theta r h^3 \partial_r h \right.$$

$$\left. + \left(\frac{11}{60} + \frac{7}{90} \theta \right) h^4 r \partial_r \theta \right) - 4\theta^2 (1 - 2\theta) \tag{E 1}$$

$$\frac{\partial \theta}{\partial t} = \frac{1}{3rh} \partial_r \left(\left(\frac{5}{4} + \frac{7}{10} \theta \right) \theta r h^3 \partial_r h \right) - \frac{\theta}{3rh} \partial_r ((1 + \theta/2) r h^3 \partial_r h)$$

$$+ \frac{\beta \theta}{rh} \partial_r \left(\left(\frac{29}{60} + \frac{23}{90} \theta \right) \theta r h^3 \partial_r h + \left(\frac{11}{60} + \frac{7}{90} \theta \right) h^4 r \partial_r \theta \right)$$

$$- \frac{\beta}{rh} \partial_r \left(\left(\frac{11}{18} + \frac{38}{105} \theta \right) \theta^2 r h^3 \partial_r h + \left(\frac{2}{9} - \frac{11}{105} \theta \right) \theta h^4 r \partial_r \theta \right)$$

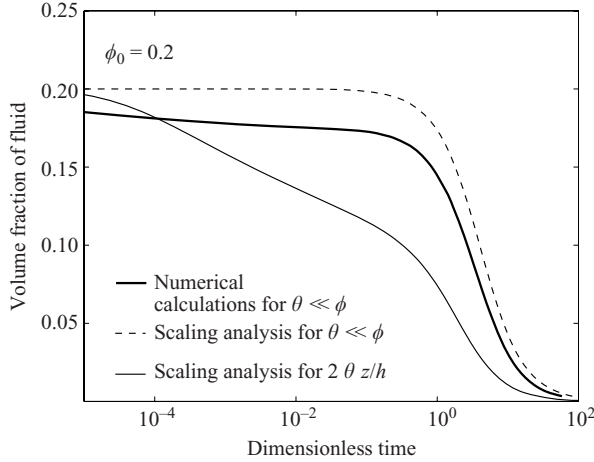$$- 4\theta^2 (1 - 2\theta) \frac{1 - \theta}{h}. \tag{E 2}$$

FIGURE 11. Evolution of the fraction of fluid as a function of time (non-dimensional). Solid line: evolution of θ for $\varphi = 2\theta z/h$. We use in that case $\partial_r h \simeq -h_s/r_s$, $\partial_r \theta \simeq 0$. Dashed line: evolution of ϕ_s obtained by scaling analysis (3.1) and (3.2), using $\varphi = \phi + (z - h/2)\theta/h$ and $\theta \ll \phi$. Bold line: numerical calculations giving the radial average $\langle \phi \rangle$ for $\varphi = \phi + (z - h/2)\theta/h$ and $\theta \ll \phi$. In all cases $\nu \ll 1$ and $\sigma \ll 1$.

We have shown in §3 that in the case of constant volume flows the volume fraction of fluid does not vary significantly with r near the centre. For simplicity, we apply the same scaling analysis to (E 1) and (E 2), i.e. $\partial_r \theta \simeq 0$, $\partial_r h \simeq -h_s/r_s$ and $V_m = \pi r_s^2 h_s (1 - \theta)$. This gives

$$d_t h_s = -\frac{\pi}{3V_m}(1 - \theta_s)(1 + \theta_s/2)h_s^5 + \frac{\beta\pi}{V_m}(1 - \theta_s)\theta_s h_s^5 \left(\frac{29}{60} + \frac{23}{90}\theta_s\right) - 4\theta_s^2(1 - 2\theta_s)$$

(E 3)

$$d_t \theta_s = -\frac{\pi}{3V_m}(1 - \theta_s)\theta_s \left(\frac{1}{4} + \frac{1}{5}\theta_s\right)h_s^4 + \frac{\beta\pi}{V_m}(1 - \theta_s)\theta_s h_s^4 \left(\frac{23}{180} + \left(\frac{38}{105} - \frac{23}{90}\right)\theta_s\right)$$

$$- 4\frac{\theta_s^2}{h_s}(1 - 2\theta_s)(1 - \theta_s).$$

(E 4)

Results of the numerical solutions to (E 3) and (E 4) in terms of evolution of average fluid fraction with time are shown in figure 11. Because the fluid fraction at the top is twice the average fluid fraction, the loss of fluid is faster than in the case of small variations of φ over z. We still observe a change in the regime when $t \simeq 1$ or $h_s \simeq 1$. Half of the fluid is lost in a period of $1T$; but the loss of fluid is complete in a comparable time of $\sim 10T$.

Initially, because of fluid and matrix mixing, a fluid fraction held constant over z is probably more relevant for natural settings. As long as the loss of fluid is not significant (i.e. $t < 1$, $h < 1$ for a Darcy flow), a constant value for φ over z is reasonable. Thus, significant fluid loss starts at $t \sim 1$ for Darcy flow, after which φ may vary significantly with z. However, regardless of this vertical variation, the total release of fluid occurs in $10T$ (for Darcy flow).

REFERENCES

BAINES, P. G. & SPARKS, R. S. J. 2005 Dynamics of giant volcanic ash clouds from supervolcanic eruptions. *Geophys. Res. Lett.* **32**, L24808. DOI:10.1029/2005GL024597.

BERCOVICI, D. 1994 A theoretical model of cooling viscous gravity currents with temperature-dependent viscosity. *Geophys. Res. Lett.* **21**, 1177–1180.

BERCOVICI, D. & LIN, J. 1996 A gravity current model of cooling mantle plume heads with temperature-dependent buoyancy and viscosity. *J. Geophys. Res.* **101**, 3291–3309.

BERCOVICI, D. & RICARD, Y. 2003 Energetics of a two-phase model of lithospheric damage, shear localization and plate-boundary formation. *Geophys. J. Intl* **152**, 581–596.

BERCOVICI, D., RICARD, Y. & SCHUBERT, G. 2001a A two-phase model for compaction and damage. 1. General theory. *J. Geophys. Res.* **106**, 8887–8906.

BERCOVICI, D., RICARD, Y. & SCHUBERT, G. 2001b A two-phase model for compaction and damage. 3. Applications to shear localization and plate boundary formation. *J. Geophys. Res.* **106**, 8925–8940.

BONNECAZE, R. T., HALLWORTH, M. A., HUPPERT, H. E. & HOGG, A. J. 1998 Axisymmetric particle-driven gravity currents. *J. Fluid Mech.* **359**, 109–142.

BONNECAZE, R. T., HUPPERT, H. E. & LISTER, J. R. 1993 Particle-driven gravity currents. *J. Fluid Mech.* **250**, 339–369.

COURANT, R., FRIEDRICHS, K. & LEWY, H. March 1967 On the partial difference equations of mathematical physics. *IBM J. Res. Develop.* **11** (2), 215–234.

CRISP, J. & BALOGA, S. 1990 A model for lava flows with two thermal components. *J. Geophys. Res.* **95**, 1255–1270.

EICHELBERGER, J. C., CARRIGAN, C. R., WESTRICH, H. R. & PRICE, R. H. 1986 Non-explosive silicic volcanism. *Nature* **323**, 598–602.

FINK, J. H. & GRIFFITHS, R. W. 1990 Radial spreading of viscous gravity currents with solidifying crust. *J. Fluid Mech.* **221**, 485–509.

FOWLER, A. C. 1984 On the transport of moisture in polythermal glaciers. *Geophys. Astrophys. Fluid Dyn.* **28**, 99–140.

GILL, A. E. 1982 *Atmosphere–Ocean Dynamics*, *International Geophysics Series*, vol. 30. Academic Press.

GRIFFITHS, R. W. & FINK, J. H. 1992 The morphology of lava flows in planetary environments: predictions from analog experiments. *J. Geophys. Res.* **97**, 19739–19748.

GRIFFITHS, R. W. & FINK, J. H. 1993 Effects of surface cooling on the spreading of lava flows and domes. *J. Fluid Mech.* **252**, 667–702.

HALLWORTH, M. A., HUPPERT, H. E. & HOGG, A. J. 1998 Effects on external flow on compositional and particle gravity currents. *J. Fluid Mech.* **359**, 109–142.

HALLWORTH, M. A., HUPPERT, H. E. & SPARKS, R. S. J. 1987 A laboratory simulation of basaltic lava flows. *Modern Geol.* **11**, 83–107.

HO, A. M. & CASHMAN, K. V. 1997 Temperature constraints on the Gingko flow of the Columbia River basalt group. *Geology* **25**, 403–406.

HUPPERT, H. E. 1982 The propagation of two-dimensional and axisymmetric viscous gravity currents over a rigid horizontal surface. *J. Fluid Mech.* **121**, 43–58.

HUPPERT, H. E. 2006 Gravity currents: a personal perspective. *J. Fluid Mech.* **554**, 299–322.

HUPPERT, H. E., SHEPHERD, J. B., SIGURDSSON, H. & SPARKS, R. S. J. 1982 On lava dome growth, with application to the 1979 lava extrusion of the Soufrière of St Vincent. *J. Volc. Geotherm. Res.* **14**, 199–222.

HUPPERT, H. E. & SIMPSON, J. 1980 The slumping of gravity currents. *J. Fluid Mech.* **99**, 785–799.

JAUPART, C. 1991 Effects of compressibility on the flow of lava. *Bull. Volcanol.* **54**, 1–9.

JOHNSON, A. M. & POLLARD, D. D. 1973 Mechanics of growth of some laccolithic intrusions in the Henry Mountains, Utah, I. Field observations, Gilbert's model, physical properties and flow of the magma. *Tectonophysics* **18**, 261–309.

KLUG, C. & CASHMAN, K. V. 1996 Permeability development in vesiculating magmas: implications for fragmentation. *Bull. Volcanol.* **100**, 58–87.

LISTER, J. R. & KERR, R. C. 1989 The propagation of two-dimensional and axisymmetric viscous gravity currents at a fluid interface. *J. Fluid Mech.* **203**, 215–249.

LLEWELLIN, E., MADER, H. M. & WILSON, S. D. R. 2002 The rheology of a bubbly liquid. *Proc. R. Soc. Lond.* A **458**, 987–1016.

MANGA, M. 1996 Waves of bubbles in basaltic magmas and lavas. *J. Geophys. Res.* **101**, 17457–17465.

MCKENZIE, D. 1984 The generation and compaction of partially molten rock. *J. Petrol.* **25**, 713–765.

NAKADA, S. & MOTOMURA, Y. 1999 Petrology of the 1991–1995 eruption at Unzen: effusion pulsation and groundmass crystallization. *J. Volcanol. Geoth. Res.* **89**, 173–196.

PATANKAR, S. V. 1980 *Numerical Heat Transfer and Fluid Flow*. Taylor and Francis.

RICARD, Y., BERCOVICI, D. & SCHUBERT, G. 2001 A two-phase model for compaction and damage. 2. Applications to compaction, deformation, and the role of surface tension. *J. Geophys. Res.* **106**, 8907–8924.

SELF, S., KESZTHELYI, L. & THORDARSON, T. 1998 The importance of pahoehoe. *Annu. Rev. Earth Planet. Sci.* **110**, 26–81.

SELF, S., WIDDOWSON, M. & JAY, T. THORDARSON A. E. 2006 Volatile fluxes during flood basalt eruptions and potential effects on the global environment: a Deccan perspective. *Earth Planet. Sci. Lett.* **248**, 518–532.

SPARKS, R. S. J., YOUNG, S. R., BARCLAY, J., CALDER, E. S., P.COLE, DARROUX, B., DAVIES, M. A., DRUITT, T. H., HARTFORD, C.,HERD, R., JAMES, M., LEJEUNE, A. M., LOUGHLIN, S., NORTON, G., SKERRIT, G., STASIUK, M. V., STEVENS, N. S., TOOTHILL, J., WADGE, G. & WATTS, R. 1998 Magma production and growth of the lava dome of the Soufrière Hills Volcano, Montserrat, West Indies: November 1995 to December 1997. *Geophys. Res. Lett.* **25**, 3421–3424.

SPIEGELMAN, M. 1993*a* Flow in deformable porous media. Part 1. Simple analysis. *J. Fluid Mech.* **247**, 17–38.

SPIEGELMAN, M. 1993*b* Flow in deformable porous media. Part 2. Numerical analysis – the relationship between shock waves and solitary waves. *J. Fluid Mech.* **247**, 39–63.

SPIEGELMAN, M. 1993*c* Physics of melt extraction: theory, implications and applications. *Philos. Trans. R. Soc. Lond. Ser.* A **342**, 23–41.

STASIUK, M. V., JAUPART, C. & SPARKS, R. S. J. 1993 Influence of cooling on lava flow dynamics. *Geology* **21**, 335–338.

SUMITA, I., YOSHIDA, S., KUMAZAWA, M. & HAMANO, Y. 1996 A model for sedimentary compaction of a viscous medium and its application to innercore growth. *Geophys. J. Intl* **124**, 502–524.

THORDARSON, T. & SELF, S. 1993 The Laki (Skatfar fires) and Grimsvotn eruptions in 1783–1785. *Bull. Volcanol.* **55**, 233–263.

TIMMERMANS, M.-L. E., LISTER, J. R. & HUPPERT, H. E. 2001 Compressible particle-driven gravity currents. *J. Fluid Mech.* **445**, 305–325.